PRINCETON UNIVERSITY

PRINCETON UNIVERSITY
DEPARTMENT OF PHYSICS

NR061-020 N6ori-105, Task II
Technical Report II-13

The Cylinder and Semicylinder in Subsonic Flow

by
Harry H. Bingham
David K. Weimer
Wayland Griffith

Submitted by
Walker Bleakney

July 1952

This work is a continuation of investigations at Princeton on the transient flow induced by a shock wave striking an object. The attempt is made to observe transition to steady conditions. The research here is related to a similar study of the cylinder in transonic flow, the subject of Mr. Bingham's senior thesis now on file in the Princeton Library.

The work is in partial fulfillment of Contract N6ori-105, Task II with the Office of Naval Research.

W.B.

THE CYLINDER AND SEMICYLINDER IN SUBSONIC FLOW

INTRODUCTION

In studying the diffraction of shock waves around various two-dimensional obstacles we have observed that flow separation and the formation of vortices contributes in an important way to transient loading of the obstacle. The cases of a cylinder and semicylinder are especially interesting because the breakaway point is not clearly defined as it is for objects having sharp corners. Accordingly a number of experiments have been made in the shock tube to observe the influence of Reynolds number and Mach number on the transient flow patterns about a cylinder and about a semicylinder mounted on a smooth plane. Some differences might be anticipated since the plane would impose a symmetry on the flow and produce a viscous boundary layer for which there is no counterpart with the cylinder.

In the course of these experiments it was noted that a condition of steady subsonic flow about both the cylinder and semicylinder was approached. Thus a comparison with von Karman's[1,2] theoretical calculation of the drag on a cylinder, from certain characteristics of its wake or "vortex street", was undertaken.

EXPERIMENTAL ARRANGEMENT

The theory and operation of the shock tube along with the technique of obtaining the density and pressure fields around a model have been well described by Bleakney, Weimer and Fletcher.[3] In brief a shock tube consists of regions of high and low pressure separated by a cellophane partition. When this diaphragm is punctured, a compression wave which rapidly steepens into a shock travels down the lower pressure section of the tube (the channel) and a rarefaction propagates up the higher pressure section (the chamber). The density field around the model due to the passage of the shock wave and the air flowing along behind it is determined by use of a Mach-Zehnder interferometer. For two dimensional flow the density change is simply proportional to the fringe shift.

The Mach number of the shock wave depends only on the initial pressure ratio across the diaphragm (if the initial temperatures are the same throughout the tube). The Mach number, pressure and density of the flow behind the shock wave (the conditions "infinitely" far from the model) are determined by the initial conditions of the gas through which the shock travels and the Mach number of the shock. The Mach number of the flow at a given point in the test section remains constant until the incident shock returns after reflection from the end of the tube.

The models used for most of the experiments reported here were a half-inch diameter polished brass cylinder squeezed between viewing windows by a rubber gasket and an equal diameter semicylinder mounted on a flat steel plate extending from the rear wall of the test section

about two feet behind the viewing windows to a point one foot upstream. The Reynolds number Re, based on cylinder diameter, varied between 10^4 and 10^5 for the range of flow speeds investigated. The time between the arrival of the incident shock and its return from the end of the tube was 1400 microseconds for the fastest flow, M=0.735 and 2200 microseconds for the lowest Mach number, 0.156. A dimensionless unit of time τ is defined as the time elapsed since the shock first struck the cylinder divided by the time to travel one cylinder diameter. Some tests were made with a 2 1/2" diameter cylinder but accurate results were limited to early flow times by the top and bottom wall interaction. For the 1/2" models no such interaction was detected. Plate I is a typical interferogram showing the disturbed fringe pattern just after the incident shock has passed the cylinder.

EQUATIONS AND SYMBOLS

To determine the density ρ at any point in the field from the measured fringe shift δ_{BA} between the initial condition A and final condition B and the initial density ρ_A we use

$$\frac{\rho_B}{\rho_A} = 1 + 0.0186 \frac{\rho_s}{\rho_A} \delta_{BA}$$

where ρ_s is the density at standard temperature and pressure and .0186 is a constant determined from the rate at which fringes pass a given point in the field of view as the pressure in the tube is varied.

The pressure p is related to the density by

$$\frac{p_B}{p_A} = \left(\frac{\rho_B}{\rho_A}\right)^{\gamma} \left(\frac{\rho_{B_o}}{\rho_{A_o}}\right)^{\gamma - 1}$$

where γ is the ratio of specific heats (for air = 7/5 = 1.4) and the subscript A_o refers to the stagnation pressure corresponding to the state A.

From the pressure field we pick out for particular attention the quantities:

$W = \frac{p_3 - p_1}{p_1}$ the overpressure on the cylinder in units of the initial pressure in the test section p_1. Subscript 1 denotes initial conditions in the test section, the subscript 2 refers to the conditions just behind the undisturbed incident shock, and subscript 3 refers to the conditions at a point in the field after the passage of the shock.

$$C_p = \frac{2}{\gamma M_2^2}\left(\frac{p_2}{p_1} - 1\right)$$ the pressure coefficient.

M_2 is the Mach number of the flow behind the incident shock.

$$C_D = \frac{1}{2}\int_0^{2\pi} C_p \cos\theta \, d\theta$$ the drag coefficient per unit length based on cylinder diameter.

For each of several sets of initial conditions we determined the variation of these quantities with τ. Figures 1a to 4f are representative of the density fields at various times for the initial conditions given on the figures. In all cases the incident shock travels to the left* The contours are lines of constant fringe shift δ_{s1}. S_I is the incident shock, S_R the shock reflected from the cylinder and S_S the portion of the incident shock which sweeps back around the cylinder. SSα is the slipstream growing from the intersection of S_I, S_R and S_{M_1}, the "Mach stem" or altered incident shock. SSβ similarly grows from the triple point of S_{M_1}, S_{M_2} (the "secondary Mach stem") and S_S.

* By accident the convention adopted in this report is just the opposite of that used in our other technical papers.

EXPERIMENTAL RESULTS

1. Cylinder with $\frac{p_2}{p_1} = 1.25$, $M_2 = .156$, Re = 32,200

Representative density fields around the cylinder for values of τ from 2.3 to 37.2 for a shock of pressure ratio 1.25 are given in Figures 1a - 1e. The variation of Cp (and W) with angle for these same times is shown in Graphs 1a - 1e respectively. In addition curves are included which exhibit the time dependence of various quantities measured from the series of Figures and Graphs. In these figures and graphs one can easily follow the decreasing pressure on the front (right) side of the cylinder from the initial head on reflection value as the reflected wave (S_R) goes out, till by Figure 1e a rather close approximation to steady potential flow[5] is in evidence. The initial high pressure on the rear due to passage of the two branches of the original shock decays more slowly than on the front so that the drag is for a short time negative (Figure 1b). Note that at this time the field is much like potential flow except that the pressures are uniformly higher. In Figure 1c we have dips in the

pressure at points A and B showing the beginnings of separation of flow and the formation of vortices. In the later pictures the growth and rearward movement of these symmetrically placed vortices can be clearly traced as they reduce the earlier high rear pressure and increase the drag. In the latest picture they have moved far enough rearward for the pressure to climb again and reduce the drag. At this stage the flow separates at 88° and the vortices are still moving back symmetrically. We expect that were we able to follow them longer we would discover a regular alternation of vortices similar to the results at $\frac{p_2}{p_1} = 1.8$ below.

2. Cylinder at $\frac{p_2}{p_1} = 1.8$, $M = .4$, $Re = 76{,}600$

Figures and Graphs 2a - 2m give our data at this shock strength. One can note again in this series a decay of the front pressure from the head on reflection value to approximately the value for potential flow. Comparisons of these results with those of the previous section show that at the higher strength, the shock sweeps more slowly around toward the front of the cylinder, and the vortices form more rapidly, in fact right behind the sweeping shock. The two sets of slipstreams SS_{α} and SS_{β} are also clearly visible. Note that the more rapid formation of vortices causes the pressure on the rear to decay much more rapidly than on the front so that on Curve 2 the drag never becomes negative. In fact, as may be seen from Curve 2 the drag reaches a maximum between Figures 2c and 2d where the vortices are growing large but are still right on the rear of the cylinder. As they move rearward (through Figure 2g) the drag drops since the pressure on the rear of the cylinder rises and is still decreasing on the front. Note in Graph 2c the small inflections at points A and B, about 100°. Perhaps these points are where the flow begins to separate from the cylinder surface. In Figure 2e, note the high pressure region where the streamlines from the two vortices meet head on. This persists through Figure 2g and similar high pressure areas may be seen later among the successive vortices. By Figure 2f the separation appears to have moved forward to points A and B, about 82° from the nose, which is consistent with the fact that the vortices have grown larger (though as they move rearward they become less deep, their depth decaying approximately exponentially with the distance from the cylinder center). In Figure 2g we can see a phenomenon unobserved in the time we had to follow the vortices produced by a 1.25 shock -- namely one vortex gets ahead and thus the force on the cylinder becomes unsymmetrical (the closer vortex exerting the greater influence). We note that in spite of the lessening influence of this farther vortex that the drag is again on the increase. This is probably due both to the beginning of turbulence preceding the formation of a third vortex, and to the continued growth of the second vortex (close one to the cylinder). Also its movement closer to the axis, causes it to exert all its influence in the horizontal direction rather than obliquely.

Seven τ later in Figure 2b we have a third vortex well formed and growing, the drag increasing still further because of it. The separation point of the flow is not apparent on the top, but on the

bottom it has remained at about 83°. From here on (Figures 2i - 2m) the vortices are shed alternately from the top and bottom of the cylinder forming examples of the Karman vortex street. As the vortices form and leave, the point of separation seems to snap back and forth, though its movement is difficult to follow clearly. The average pressure drag coefficient remains at about 1.5 from $\tau = 30$ on.

An example of the origin of fluctuations observed at later times is shown in Figure 2k. The fifth vortex has moved down almost to the axis so that the rear pressure has dropped far below its average value, causing a sharp peak in the drag curve. All the data available are consistent with the assumption that similar maxima in drag are associated with each vortex leaving the cylinder so that it is subject to a periodic horizontal and vertical force. Curve 2a has been drawn on this basis even though insufficient points are available to fully justify such a procedure.

The pressure at the nose and at 45° intervals around the cylinder is plotted as a function of time in Curves $2\alpha_1$, and $2\alpha_2$ with a detail of early times in Curve $2\alpha_3$. The initial values are calculated as follows: for the front from the pressure due to reflection of the shock; for 45°, 90°, 135°, using the appropriate pictures in Reference 4 (No. 508, No. 405); for 180° from measurement of δ on a picture taken especially for the purpose. The pressure on the front may be seen to approach approximately the stagnation pressure value. At 45° the pressure is about 30% too high for potential flow, at 90° about two and a half times as high as potential flow, at 135° about 15% lower and 180° about half the potential flow value. The discontinuities in Curves $2\alpha_1$ - $2\alpha_3$ (e.g., at τ 2.2 on the 135° Curve) are due to the passage of the sweeping shock S_S. Its decay as it moves forward from the rear of the cylinder may be followed in the several curves. The fluctuations in pressure on the cylinder rear due to the formation and shedding of vortices may be clearly followed in the curves for 135° and 180° and to some extent for 90°. We will consider these curves further in comparison with the semicylinder results.

Similar results with respect to drag, pressure curves and vortex street were obtained for some series shot at approximately the same Mach number but different Reynolds numbers. A few of these results are marked (+) on Curve 2a.

The existence of well formed vortex streets suggested comparison with von Karman's theory[1,2]. An analysis of the stability of various conceivable configurations of vortex trails led von Karman to the conclusion that the only stable configuration is the assymmetrical type with

$$\frac{h}{l} = \frac{1}{\pi} \coth^{-1}\sqrt{2} = .281$$

He also found an expression for the drag D on the cylinder per unit

length in terms of the strength of the vortices Γ, the density ρ, the free stream velocity V, the vortex velocity relative to the stream u, and the ratio h/l:

$$D = \rho \Gamma \frac{h}{l}(V - 2u) + \rho \frac{\Gamma^2}{2\pi l}$$

Where

$$u = \frac{\Gamma}{2l} \tanh \frac{\pi h}{l} = \frac{\Gamma}{2\sqrt{2}\, l}$$

Using

$$C_D = \frac{D}{\frac{1}{2}\rho d V^2}$$

we can reduce the above expression to

$$C_D = \frac{l}{d}\left[1.59 \frac{u}{V} - 0.63 \left(\frac{u}{V}\right)^2\right]$$

Measurement of Figures 2a - 2n and others not included here gives $h/l = 0.310$ for all vortices and $h/l = 0.272$ for those beyond about one diameter from the cylinder. This is in good agreement with the theory. The ratio l/d of vortex separation to cylinder diameter is 3.14.

To find a drag coefficient from the theory an estimate must be made of the speed of the vortex centers as well. The points on Curve 2β represent the positions of the various vortices appearing in each picture plotted against the τ of that picture. For example, the three vortices of Figure 2h are represented by points above $\tau = 28.65$ at the height corresponding to their respective distances from the cylinder center. Since each picture represents a separate experiment in the shock tube it is sometimes difficult to tell whether the top or bottom vortex left the cylinder first. All of the Figures 2a - 2m have been oriented so that the first vortex left the top according to our best guess. The numbers on the drag maxima in Curve 2α as measured from the pressure are assigned accordingly.

The path of each vortex may be traced fairly unambiguously in Curve 2β. An idea of the reproducibility of the experiments may be seen in the two sets of points at $\tau = 62$ which come from separate firings of the tube. The four symbols o ρ q δ represent series taken under slightly different conditions of temperature and humidity.

Values for the vortex velocity can be obtained from Curve 2β. The average slope of the lines drawn gives $u' = 0.240$ times the shock velocity. Since the velocity V of the free stream with respect to the body is 0.338 times the shock velocity we find $\frac{u}{V} = \frac{V - u'}{V} = .290$. Substitution in the formula gives $C_D = 1.28$ which is in fair agreement with the value 1.5 determined from an average of Curve 2a.

A periodic lift force also acts on the cylinder as vortices are shed. This force has half the frequency of the fluctuations in drag since every other vortex leaves a given side of the cylinder. Sufficient experimental points have not been obtained to trace through

this variation completely but all those available are consistent with the assignment of vortices shown in Curve 2a. Values of lift coefficient vs. τ are plotted in Curve 2b. The solid line should not be taken seriously, it is only drawn as a qualitative suggestion. During early stages the flow is symmetrical and the lift negligible. After $\tau = 20$ oscillations build up to magnitudes of $C_L \sim 0.9$. So far as we know this has not been measured before because the shedding frequency is too fast for response by a wind tunnel lift balance. Measurement with a strain gauge would presumably yield results on the fluctuations as well as on the average values.

3. Semicylinder at $\frac{p_2}{p_1} = 1.8$, $M = 0.4$, $Re = 76{,}000$.

As might have been expected, the density field around a semicylinder is essentially the same as for a cylinder during the early stages of flow. Even when the flow about the cylinder has become unsymmetrical, (Figures 3d, 3e) certain portions of the patterns are qualitatively similar, including the high pressure region A where a stagnation point forms on the plate in somewhat the way one forms behind the two vortices in Figures 2e, 2f. The corner between the plate and the semicylinder rear forms a better trap for still air than the unprotected rear of the cylinder, however, so the pressure remains systematically higher behind the semicylinder than behind the cylinder. Thus the measured drag on the semicylinder shown in Curve 3 has an average value $C_D = 0.90$ compared to $C_D = 1.5$ for the cylinder.

At the later times the pattern is no longer always even qualitatively similar. For example, in Figure 3f, $\tau = 23.4$ the second vortex is already well formed while the first is apparently beginning to break up. Figure 2g for the cylinder, ($\tau = 21.5$), on the other hand shows both vortices still well formed moving together, and little sign of a third vortex (which would correspond to the second on the semicylinder). In Figure 3g ($\tau = 30.2$), the second vortex has grown larger and moved back allowing the drag to further decrease. The positions of the first and second vortices in this picture correspond roughly to the first and second from the upper surface of the cylinder (i.e., the first and third) in Figure 2h ($\tau = 28.65$). The pressure distributions over the rear in Graphs 3g and 2h are quite different because the vortices cannot grow as large behind the semicylinder before being swept away as they can behind the full cylinder.

In Figure 3h we have what seems to be the third vortex still growing and then another maximum in the C_D curve. By Figure 3i the third vortex has pretty well gone so the drag is again low. In these pictures the position of the point of separation of the flow from the cylinder surface seems to be further back than in set 2, in accord with the smaller vortices. No separation point further forward than 86° was noted.

That three vortices form by $\tau = 50$ would be suspected from the behavior of the whole cylinder, from which the sixth vortex is de-

veloping by $\tau = 50$. That each vortex would form on the semicylinder somewhat sooner than the corresponding vortex on, say, the top of the whole cylinder is also to be expected since there would be no vortex from the bottom to interfere. Understandable also is the more rapid breakup of the semicylinder vortices due to the influence of the plate.

Some insight into the origin of the differences in drag between the cylinder and semicylinder may be gained by studying the variation of pressure with time for the locations shown in Curves $2\alpha_1$ - $2\alpha_3$. The pressure on the front is seen to approach the stagnation pressure about as fast in both models even though a boundary layer forms along the plate ahead of the semicylinder. At 45° the pressure is uniformly the same in the two models over the time range studied within experimental error. At 90° a slightly higher pressure appears after $\tau = 20$ or so. This probably arises because of the smaller size of the vortices shed from the semicylinder. At 135°, though again the differences before $\tau = 20$ are not significant, the later times show clearly that the pressure on the semicylinder is always higher than on the whole cylinder. This again is because the vortices are not so large, i.e., because there is a region of dead air which the plate protects from being swept away. The curve for 180° shows clearest of all the presence of this high pressure region. There seems also to be a difference between the pressure on the rears of the two models between $\tau = 5$ and 10, possibly because of the difference in the manner of growth of the first vortices in the two cases.

4. Cylinder at $\frac{p_2}{p_1} = 3.0$, $M = .735$, $Re = 30,800$

As the flow Mach number is increased, more and more phenomena resulting from the compressibility of the air begin to appear. Some highly interesting effects adjacent to regions of locally supersonic flow may be seen in Figures 4a - 4d.

In Figure 4a for example we note that the sweeping shock seems to be having difficulty going back upstream around the cylinder, having reached only some 107° in $\tau = 4.76$ (compare Figure 2c where in $\tau = 5.1$ the shock is just about at the cylinder nose, some 95° further). The vortices, too are forming more rapidly and have developed little shock waves like horns on their sides away from the axis. The slip streams are again visible along with the reflected and sweeping shocks.

The next picture (Figure 4b) shows the sweep shock having given up trying, in fact to have been partly swept away itself (S_A between the two vortices) and the rest of it curled past the cylinder. The drag has dropped nearly 40% due to the decay of the reflection high in the front and the rapid removal of the first two vortices (which still have their horns). Figure 4c shows the remnants of the sweep shock still being taken slowly back by the flow, while two new shocks (A and B on graph and figure) appear about $\pm 75^\circ$ from the cylinder nose. The vortices with their horns still move back, the rear pressure continues to rise and the drag

to drop.

Later, we find the sweep shock disappears entirely and regular alternation of vortices takes place. These vortices have horns till they are a diameter or two back of the cylinder, by which time they have widened out so that they no longer have regions of supersonic rotational velocity and the horns have disappeared. An example of the later appearance of the flow is Figure 4d which shows the assymmetrical character of this flow due to the formation of vortices. We did not take enough pictures to follow the drag fluctuations in detail or to check the Karman C_D prediction. The points we have form a smooth curve suggesting that the fluctuations in the drag with time are not large. The drag coefficient, as may be seen from Curve 4, rises as the later vortices are formed and shed and reaches a value of 2.2 at $\tau = 60$. From what pictures we have we found that λ/l .276 (including all vortices) suggesting, perhaps that with increasing Mach number λ/l decreases.

In all of the analysis a tacit assumption has been made that the flow patterns observed are accurately two-dimentional. Previous experience supports this idea since the boundary layer which forms on the side walls of the tube is very thin compared to the 4" tube width. Because the shock and slipstreams observed in this group of experiments appear sharp in the pictures it also seems reasonable to assume that the flow past the 1/2" diameter cylinder is actually two-dimensional over the 4" span.

CONCLUSIONS

Our expectation that the flat plate would affect the transient and steady flow pattern around a cylindrical obstacle was borne out by experiments with shock waves of $p_2/p_1 = 1.8$. In particular it was found that the rearward extending plate protected a high pressure "dead air" region behind the cylinder, which lowered considerably its drag as compared to a free cylinder.

Fluctuations in the pressure drag coefficient with the formation and shedding of vortices alternately from the top and bottom of the free cylinder were found to be on the order of $\pm$ 20% from the mean value of 1.5 (for Mach number 0.40, Reynolds number 76,000). Similar results were also obtained for Reynolds numbers from 12,000 to 86,000 at approximately this Mach number. Our data suggest but are insufficient to prove, that there is little variation of the average drag coefficient within this range of Reynolds numbers for Mach number 0.40. The lift coefficient varies over about $\pm$ 0.9 with half the frequency of the drag fluctuations.

The presence of the plate upstream from the semicylinder was found to have little detectable effect. Downstream, however, somewhat higher pressures were observed and the drag coefficient was reduced to about 0.90.

von Karman's theory for the stable configuration of the wake

of vortices behind the cylinder was approximately verified, not only for Mach numbers around 0.4, Reynolds numbers in the range 10^4-10^5 but for a few cases of Mach number as high as 0.73 (Reynolds number 31,000). At M = .40 λ/ℓ was found to be .272 as compared with a predicted value .281.

Calculation of the drag coefficient from the character of the vortex street according to von Karman's theory was found to give a value for $C_D = 1.28$. No wind tunnel experiments of which we are aware have been done for these conditions. Several investigators [6] have studied this range of Reynolds number at very low Mach numbers and agree on $C_D \approx 1.2$.

Supporting experiments at Mach numbers 0.16 revealed flow patterns qualitatively similar to potential flow, but with the pressure uniformly higher. These flow patterns persist for only a few shock crossing times before the flow begins to separate and form vortices. At higher Mach numbers the vortices form so quickly that a pattern similar to potential theory is never observed. The vortex center depth was found to decay approximately exponentially with distance from the cylinder center.

The experiments at Mach number 0.73 revealed complex interactions between the flow and the various diffracted shock waves. The presence of locally supersonic flow was indicated by shock waves attached to the cylinder surfaces and to vortices close to the cylinder.

REFERENCES

1. T. von Karman, Göttinger Nachrichten, 509-517, 1911; 547-556, 1912. von Karman and Rubach, "Uber den Mechanismus des Flussigkeits -- und Luftwiderstandes, Phys. Zeits.13, 49, 1912.

2. C. N. H. Lock, "On the System of Vortices Generated by a Circular Cylinder in Steady Motion Through a Fluid", Phil. Mag., 6th series, 50, 1083, 1925.

3. Bleakney, Weimer, Fletcher, "The Shock Tube, a Facility for Investigations in Fluid Dynamics, Rev. Sci. Inst. 20, 807. 1949.

4. Bleakney, White, Griffith, "Measurements of Diffraction of Shock Waves and Resultant Loading of Structures", Jour. App. Mech. 17, 439, 1950.

   "The Diffraction of Shock Waves Around Obstacles and the Transient Loading of Structures", Princeton University Technical Report N6 ori-105 Task II, No. II-3.

5. See for example W. F. Durand, Aerodynamic Theory, GALCIT 1934, Vol. I, p. 155

6. For references to literature on cylinder drag at low Mach numbers, see S. Goldstein, Modern Developments in Fluid Dynamics, Oxford 1938, especially section 184 in Chap. IX and Chap. XIII and II.

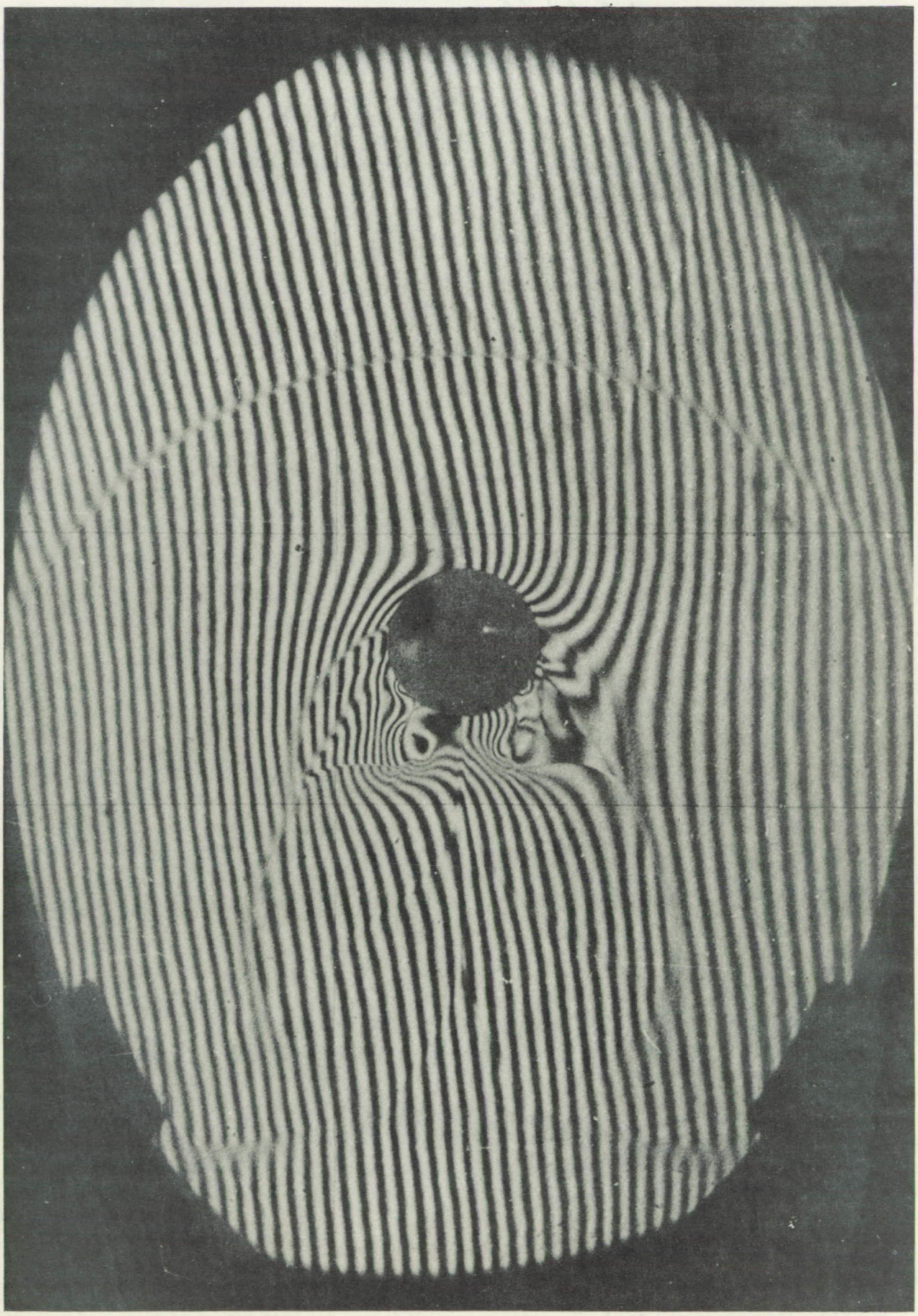

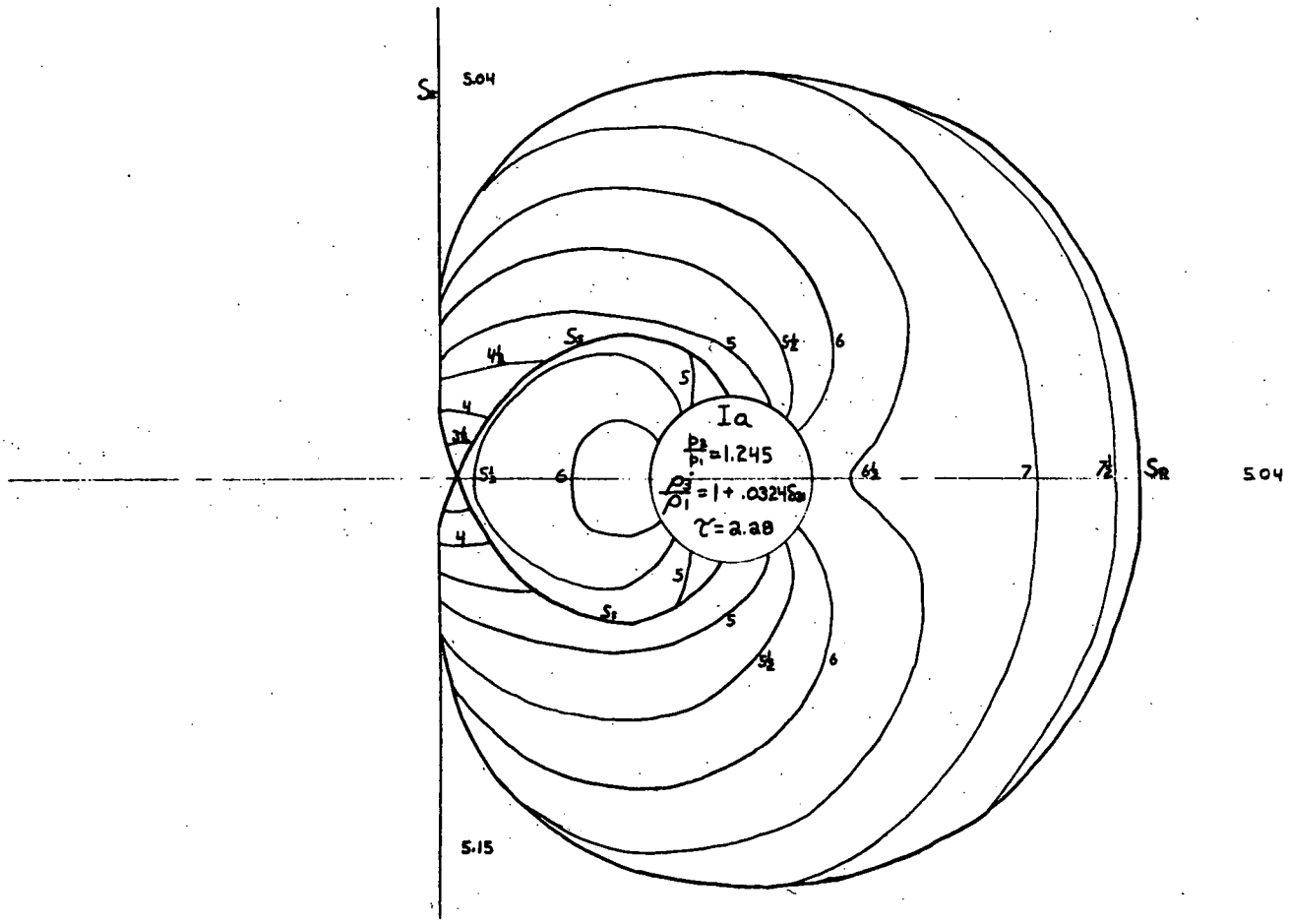
Ia
$\frac{p_2}{p_1} = 1.245$
$\frac{\rho_2}{\rho_1} = 1 + .03245\varepsilon_{20}$
$\gamma = 2.28$
5.04
5.15

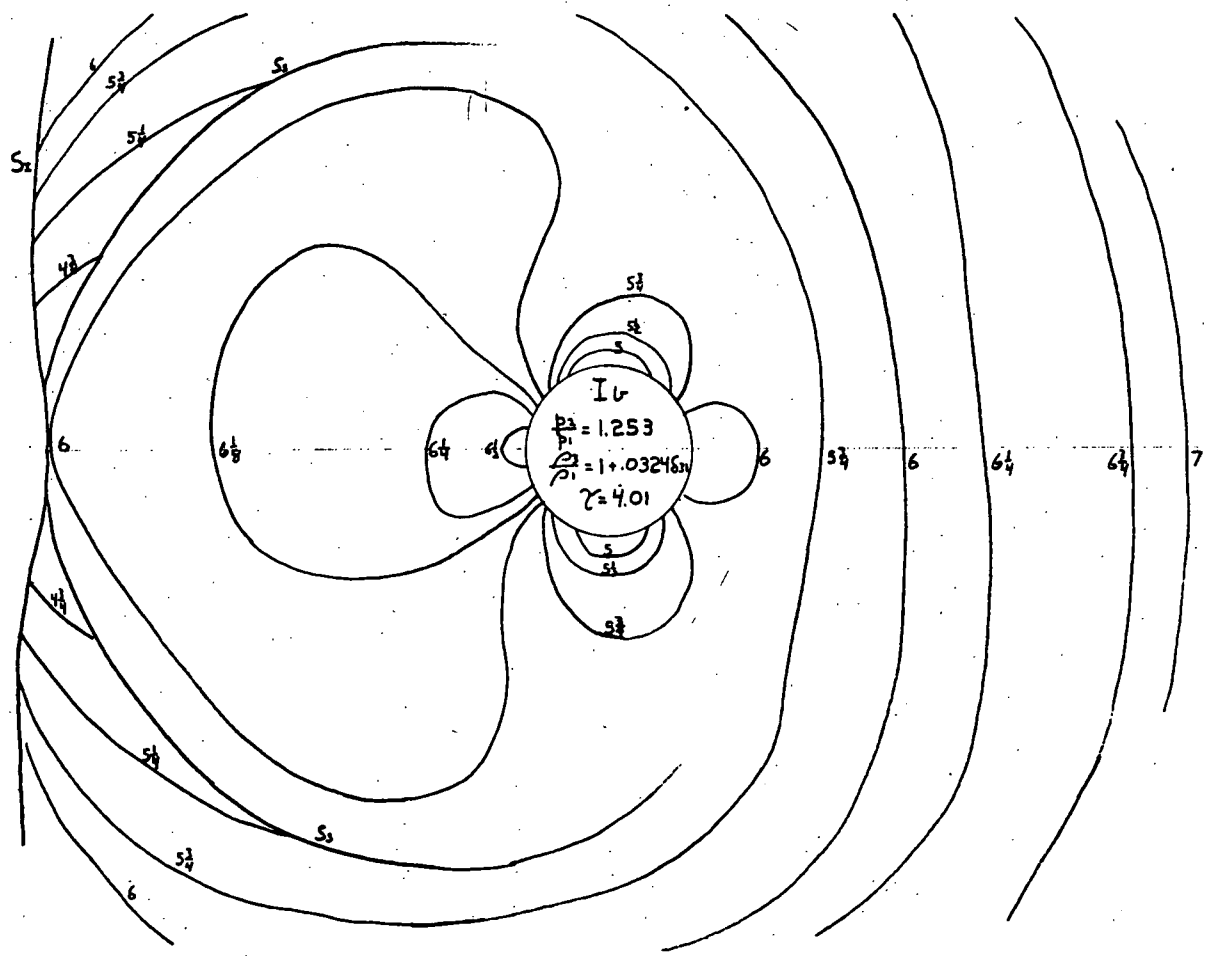
Ib
$\frac{p_3}{p_1} = 1.253$
$\frac{\rho_3}{\rho_1} = 1 + .03246\varepsilon_{31}$
$\gamma = 4.01$

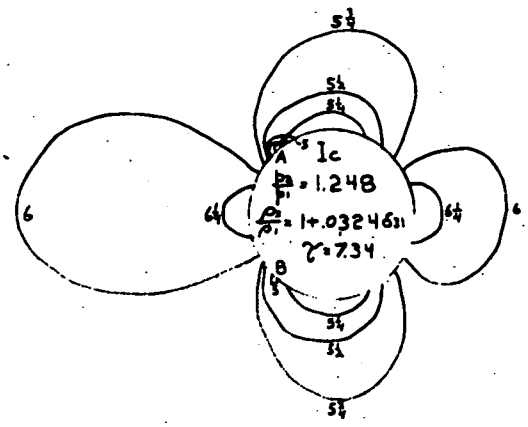
Ic
$\frac{p_2}{p_1} = 1.248$
$\frac{\rho_2}{\rho_1} = 1 + .032463$
$\gamma = 7.34$
A
B

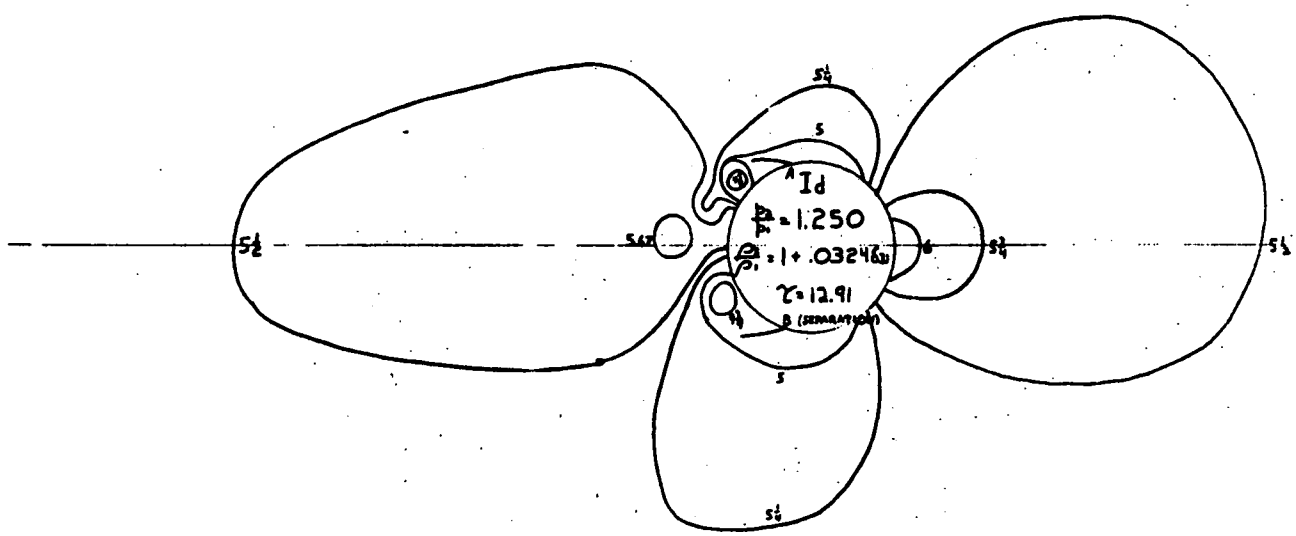
Id
$\frac{p_2}{p_1} = 1.250$
$\gamma = 12.91$
A
B (SEPARATION)

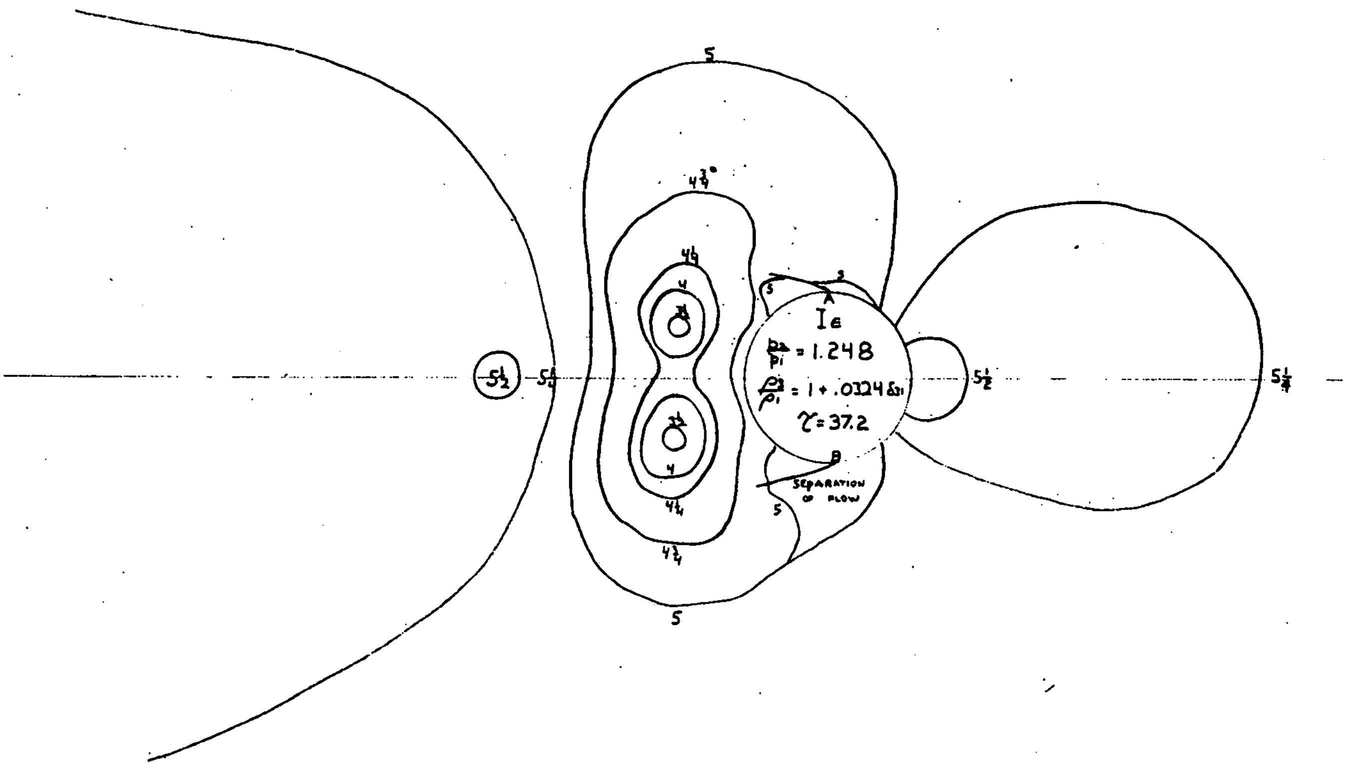

5
$4\frac{3}{4}$°
$4\frac{1}{4}$
4
I E
$\frac{p_2}{p_1} = 1.248$
$\frac{\rho_2}{\rho_1} = 1 + .0324\delta_{21}$
$\gamma = 37.2$
A
B
SEPARATION OF FLOW
$5\frac{1}{2}$
$5\frac{1}{4}$

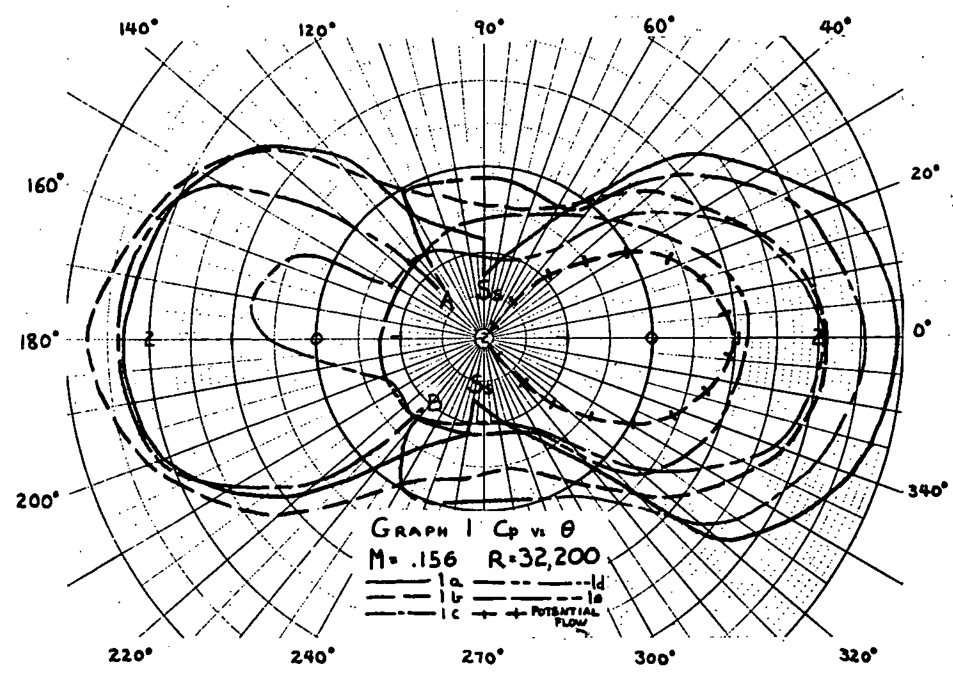

140°
120°
90°
60°
40°
20°
160°
180°
0°
200°
340°
220°
240°
270°
300°
320°
A
B
GRAPH 1 Cp vs θ
M = .156 R = 32,200
1a
1b
1c
1d
1e
POTENTIAL FLOW

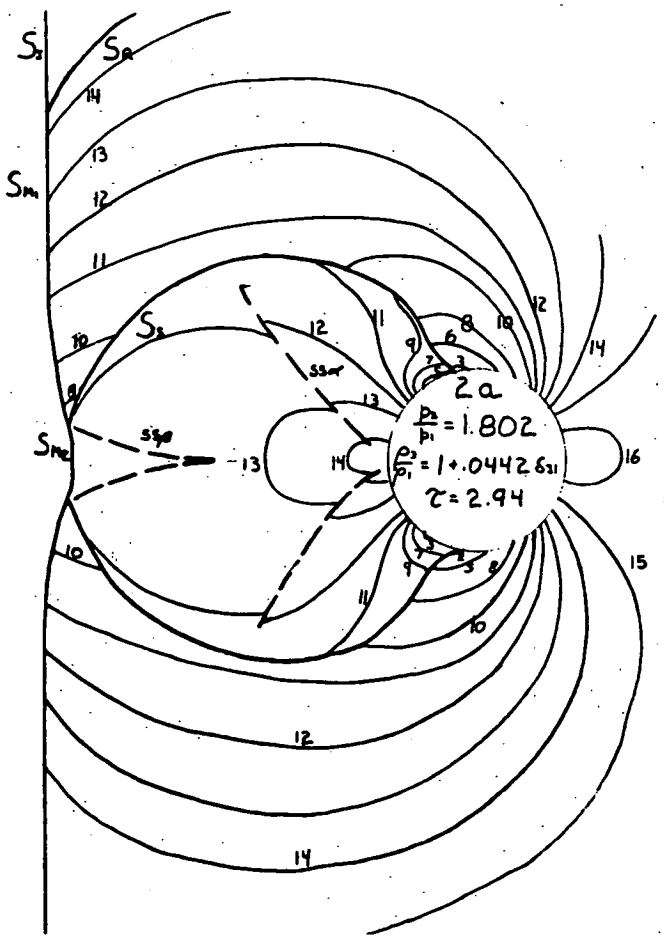
2a
$\frac{\rho_2}{\rho_1} = 1.802$
$\frac{\rho_3}{\rho_1} = 1 + .0442\,\delta_{31}$
$\tau = 2.94$

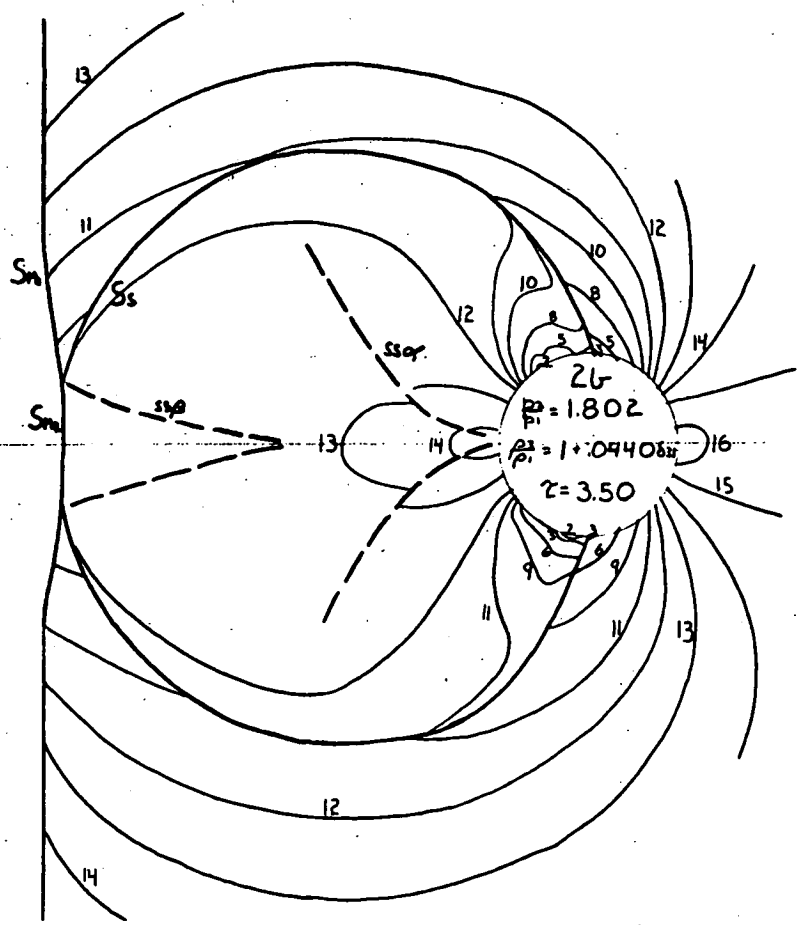
2b
$\frac{\rho_2}{\rho_1} = 1.802$
$\frac{\rho_3}{\rho_1} = 1 + .0440\,\delta_{31}$
$\tau = 3.50$

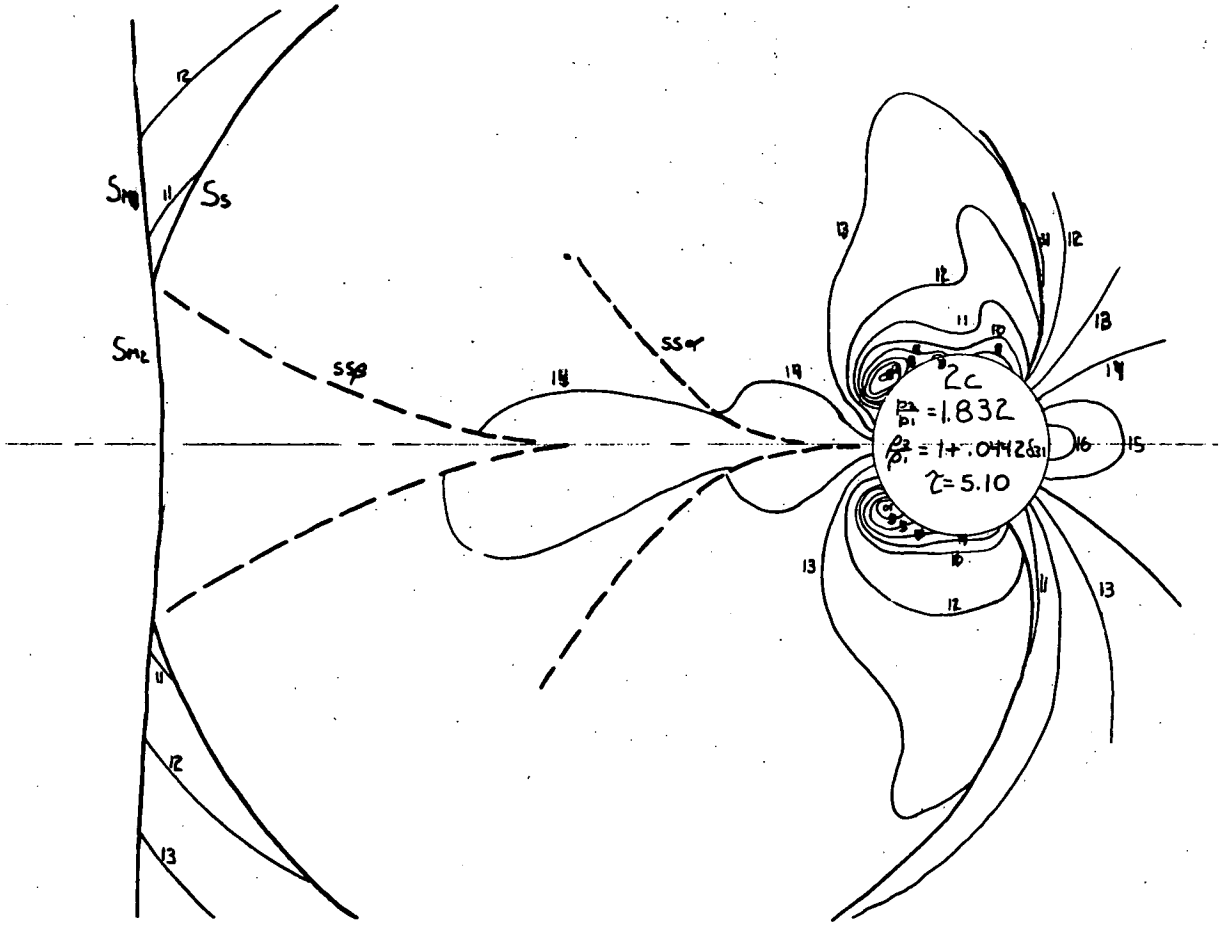
Sm1
Ss
Sm2
SSβ
SSα
2c
p2/p1 = 1.832
ρ2/ρ1 = 1+.0442δ31
τ = 5.10

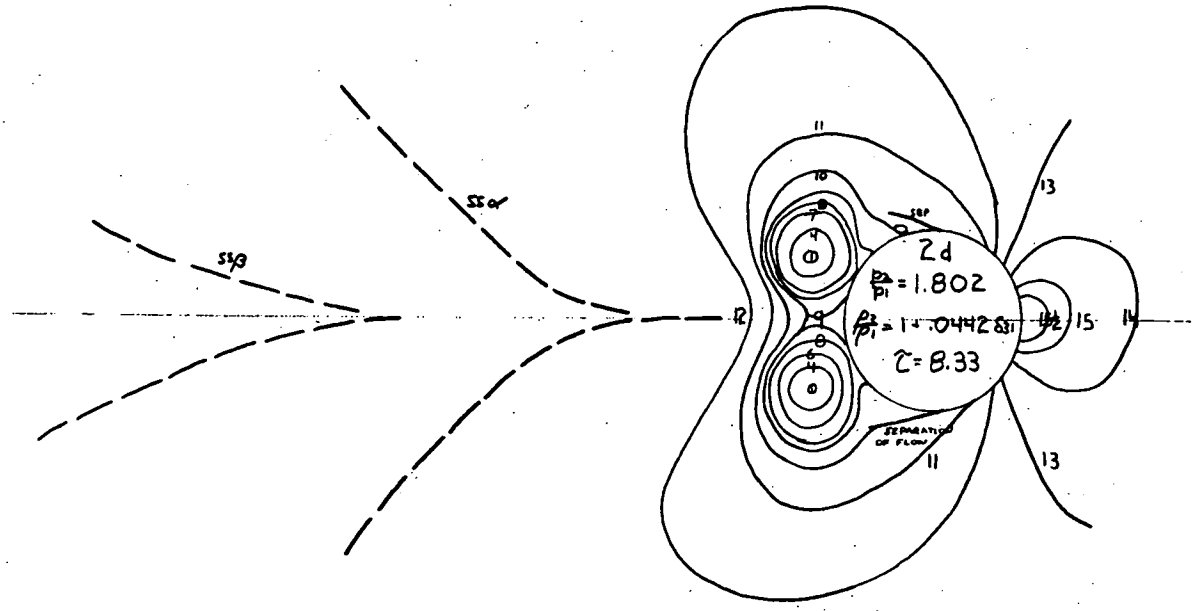
SSα
SSβ
2d
p2/p1 = 1.802
ρ2/ρ1 = 1+.0442δ31
τ = 8.33
SEPARATION OF FLOW

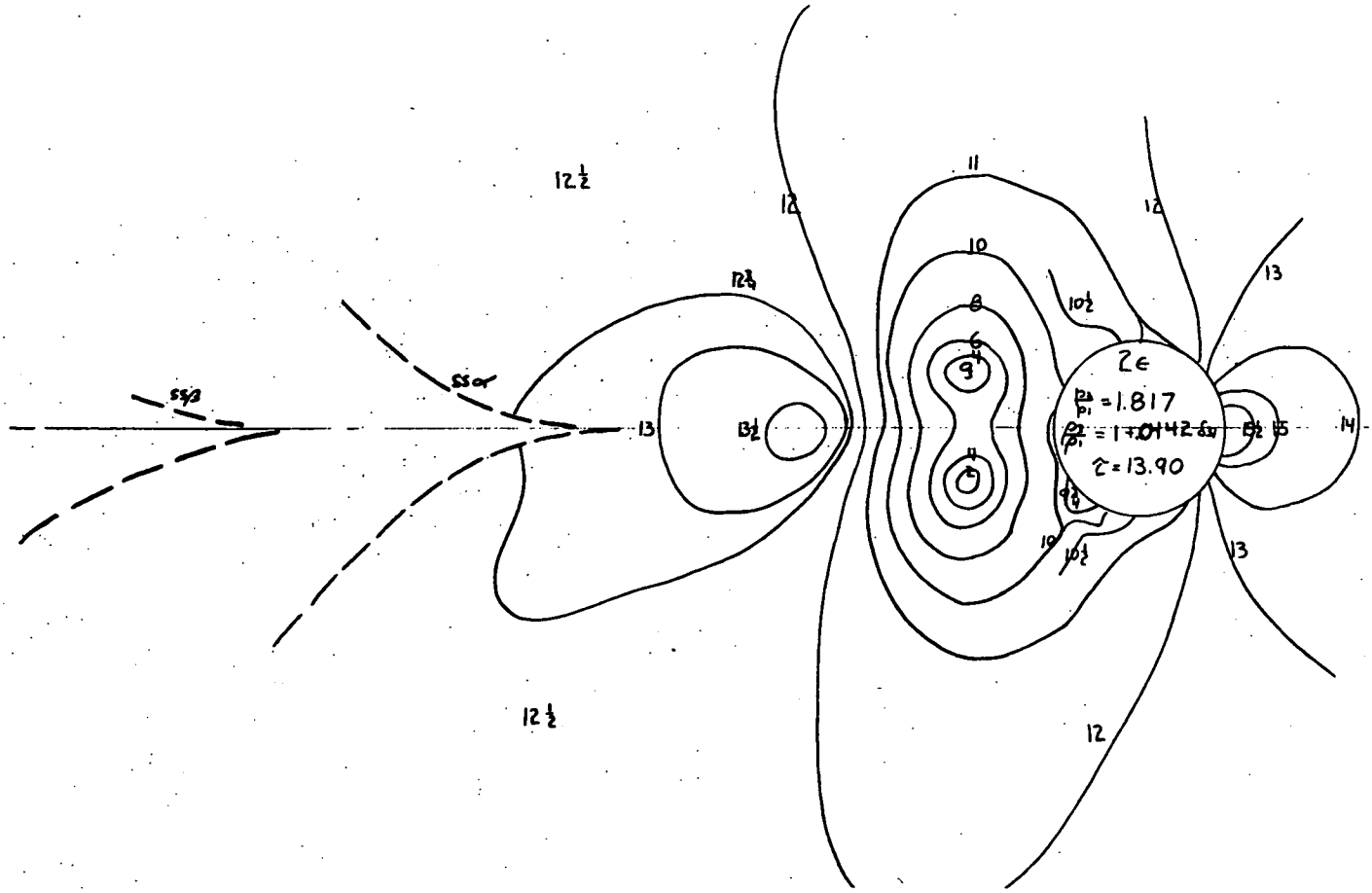
12½
12¾
11
12
10
8
6
9
11
10½
13
2e
$\frac{p_2}{p_1}$ = 1.817
$\frac{\rho_2}{\rho_1}$ = 1+.0142 δ_{21}
τ = 13.90
13½
15
14
10
10½
13
12½
12
SSW
SSW
13

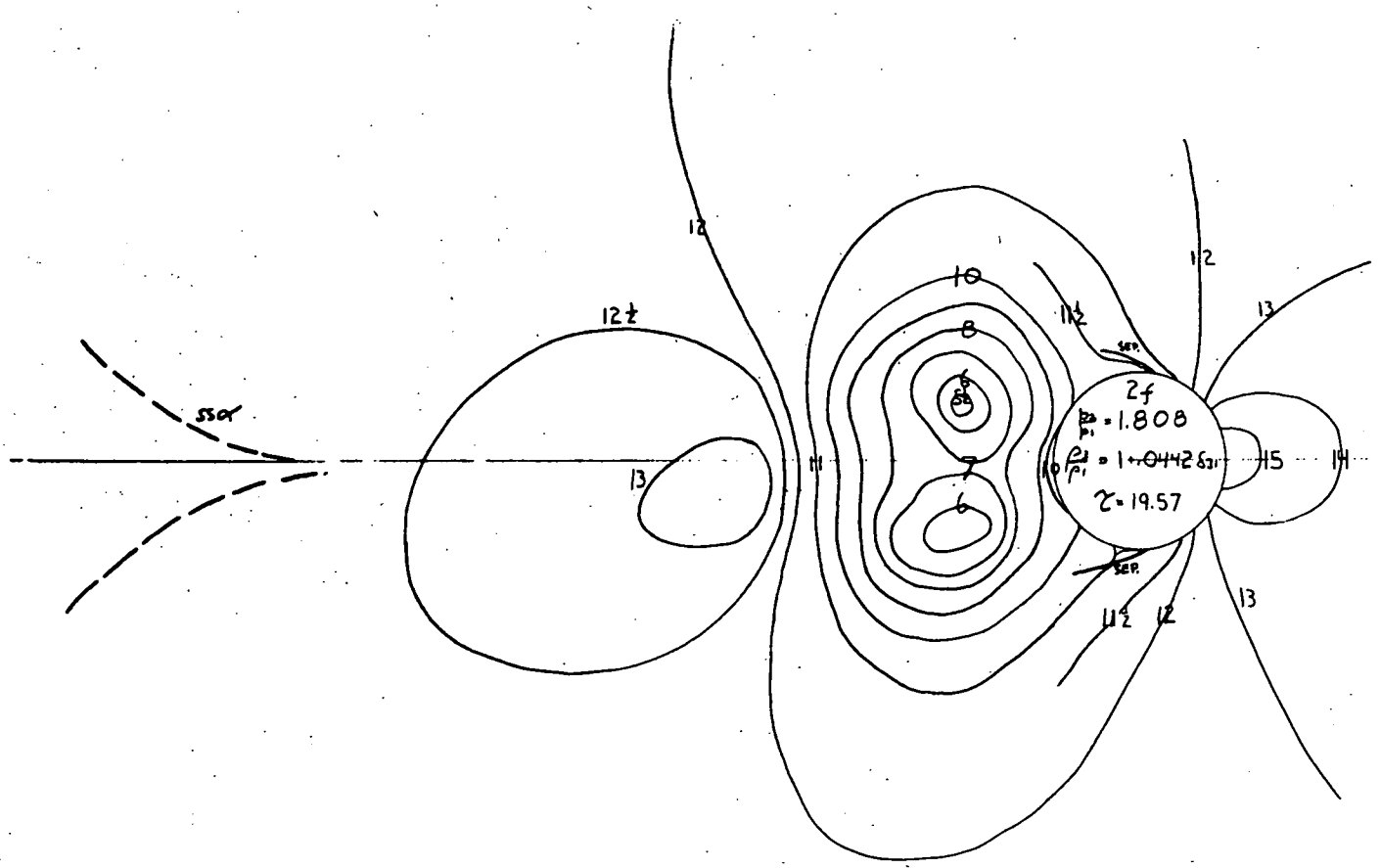
12
10
12½
8
11½
12
13
SEP.
6
2f
$\frac{p_2}{p_1}$ = 1.808
$\frac{\rho_2}{\rho_1}$ = 1+.0142 δ_{21}
τ = 19.57
15
14
SSW
13
11
10
7
6
SEP.
11½
12
13

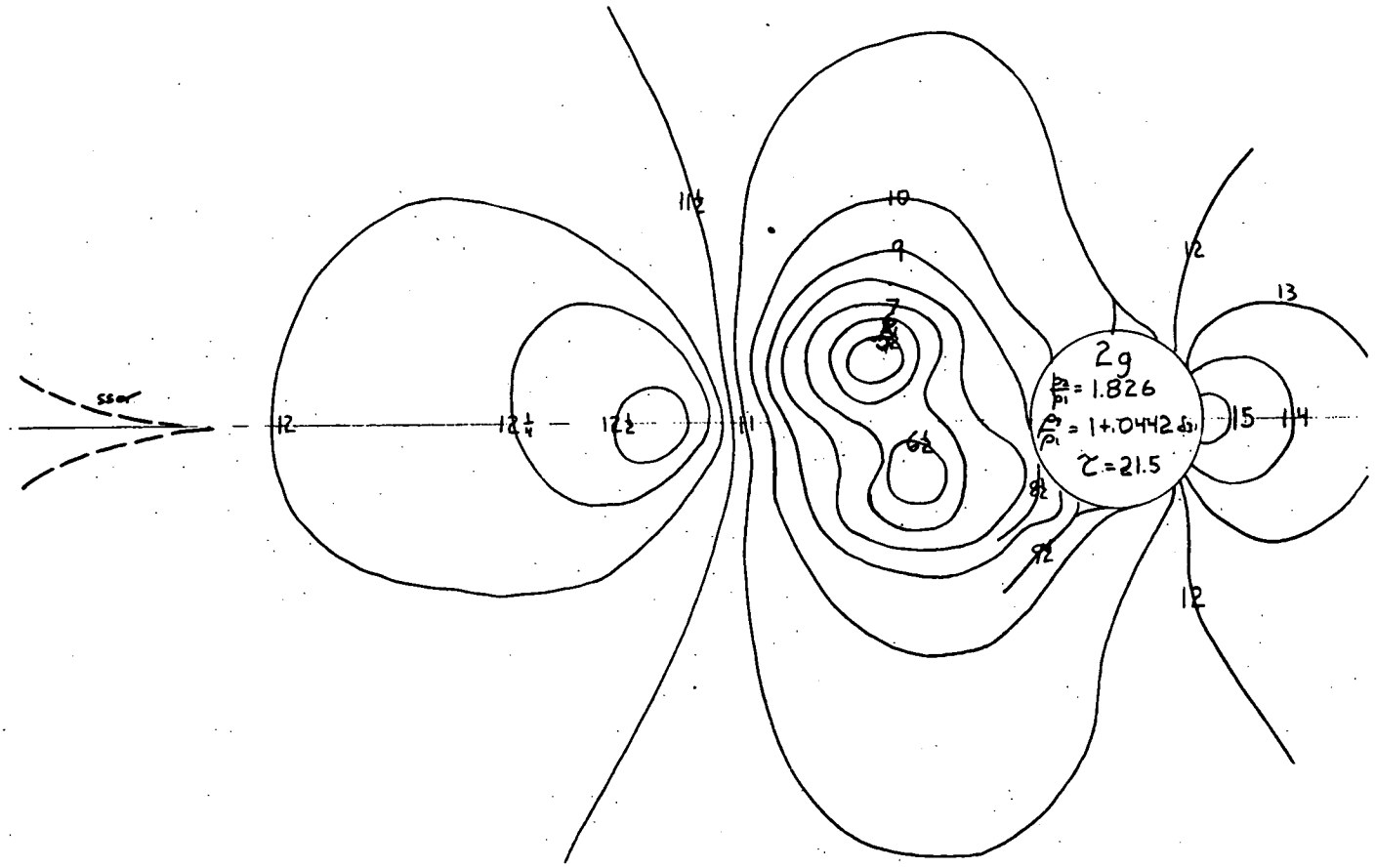
2g
$\frac{p_2}{p_1}$ = 1.826
$\frac{\rho_2}{\rho_1}$ = 1+.0442 δ_1
τ = 21.5
sonic

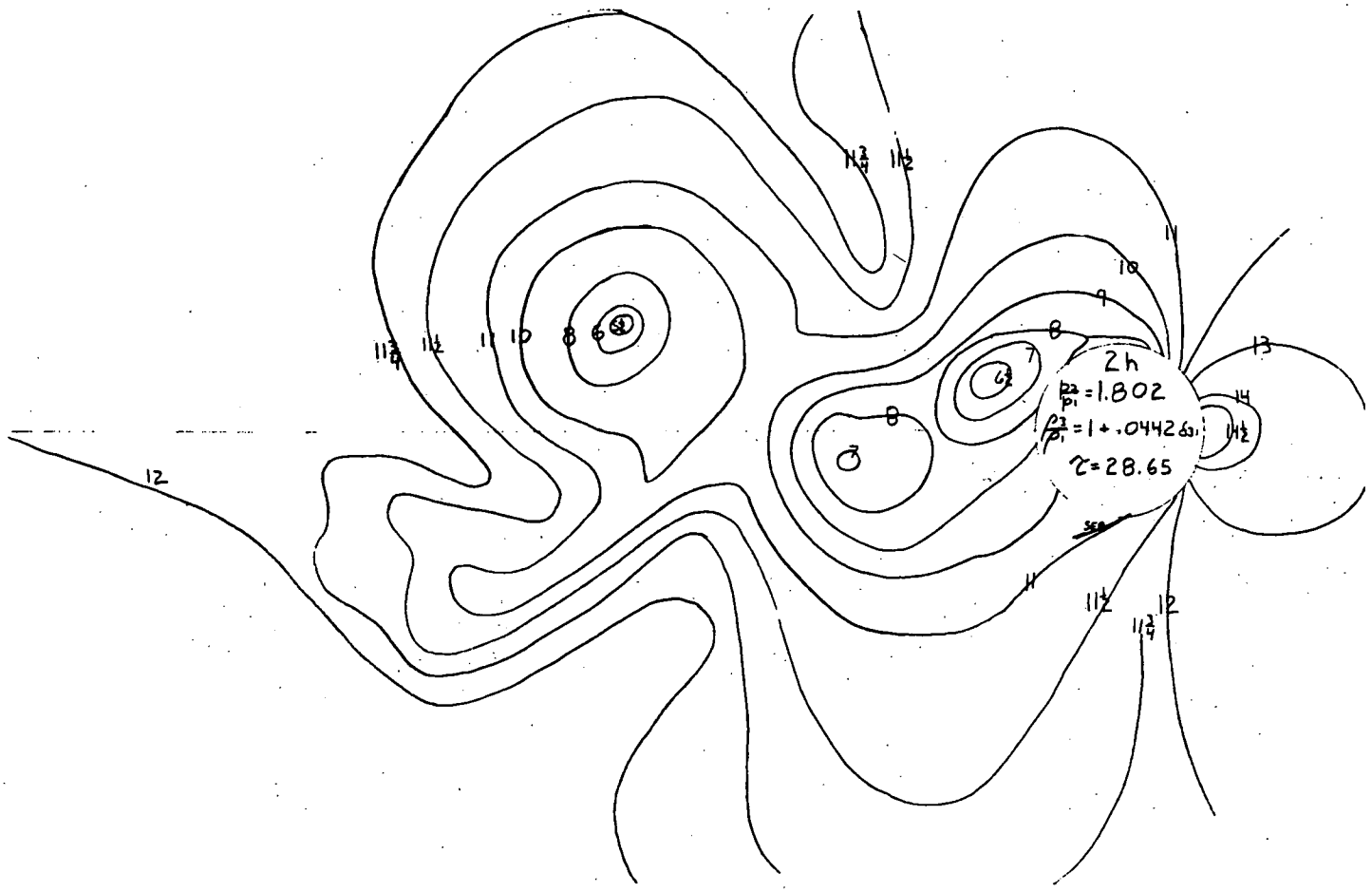
2h
$\frac{p_2}{p_1}$ = 1.802
$\frac{\rho_2}{\rho_1}$ = 1+.0442 δ_1
τ = 28.65
sonic

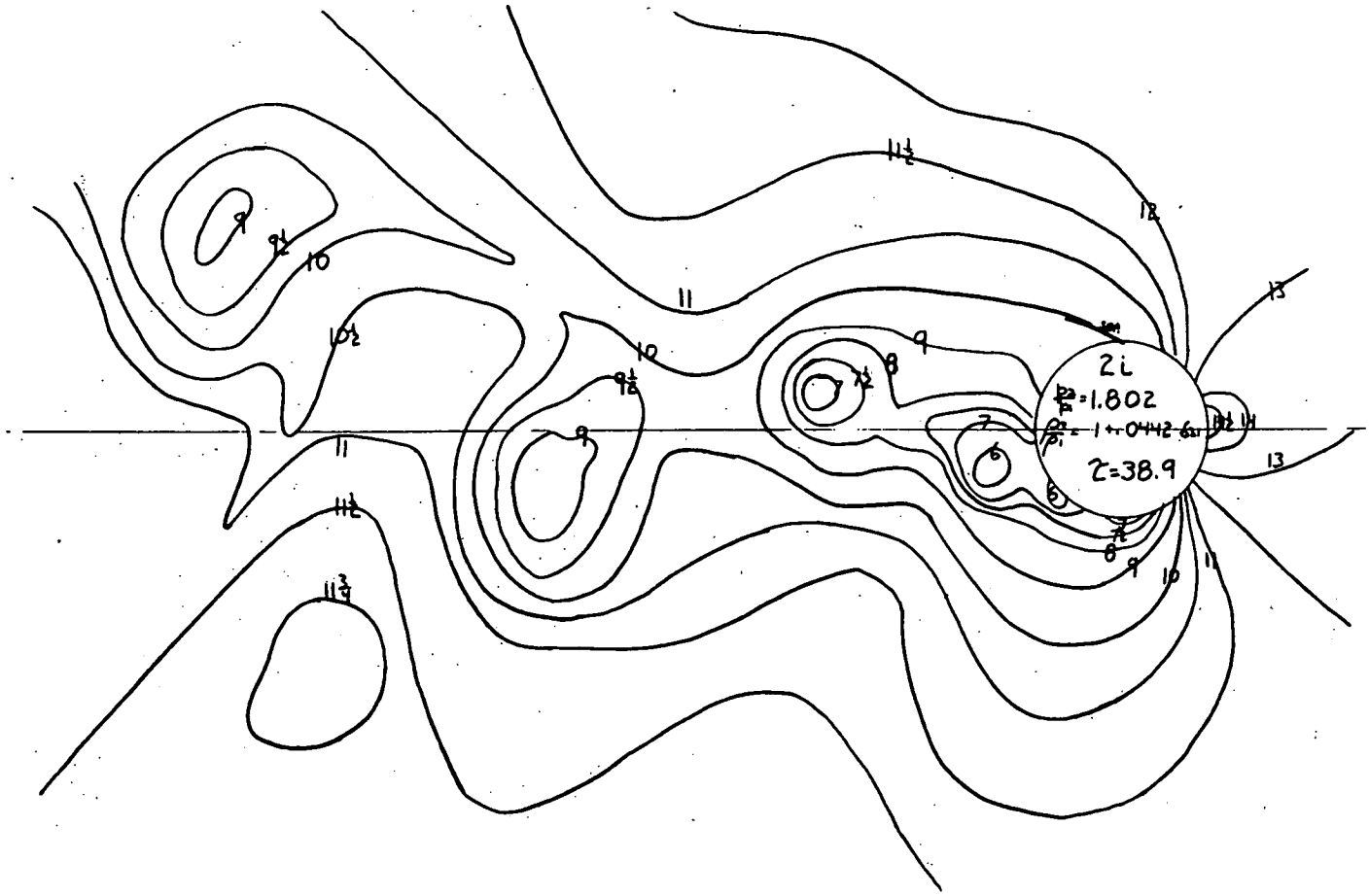
2i
$\frac{p_2}{p_1}$ = 1.802
$\frac{\rho_2}{\rho_1}$ = 1 + .0442 6u
τ = 38.9

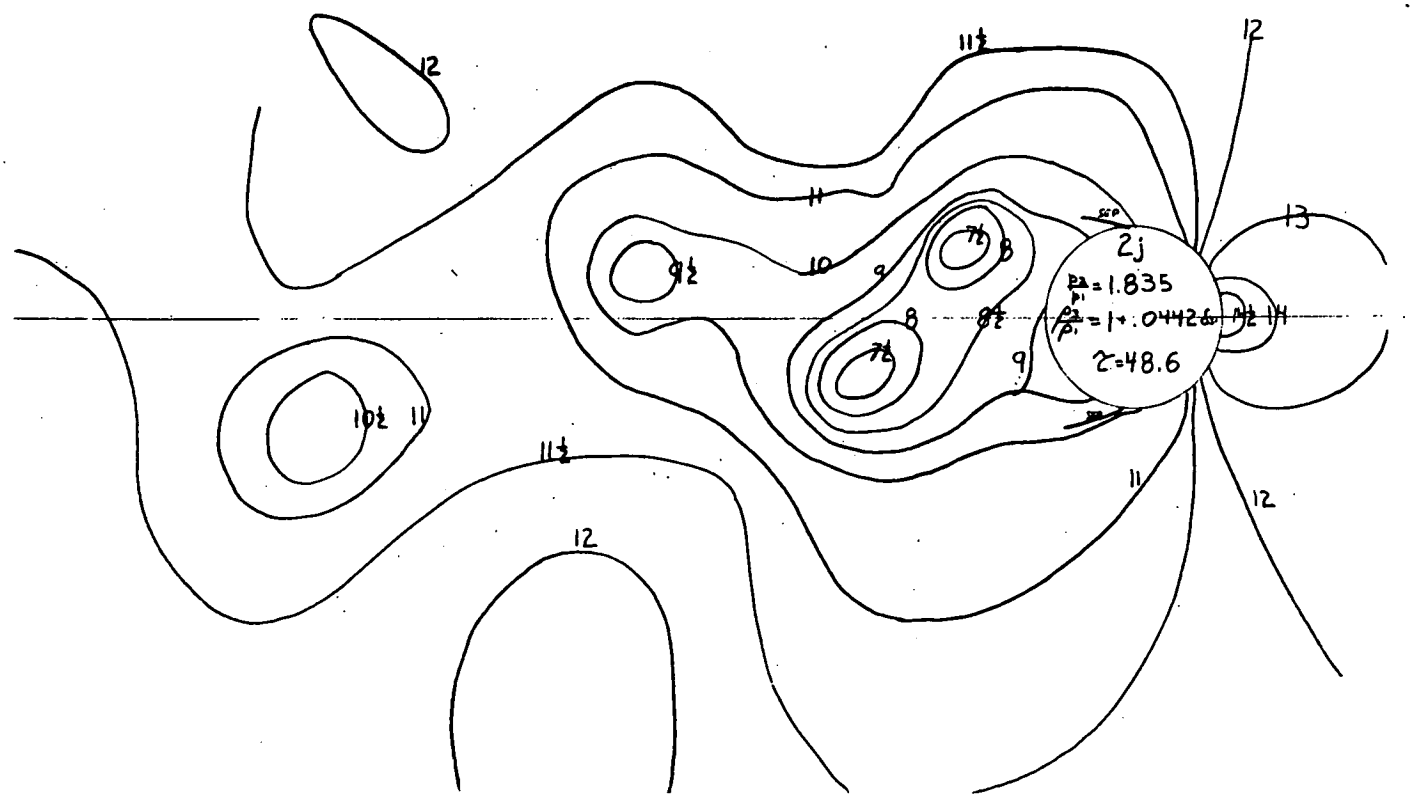
2j
$\frac{p_2}{p_1}$ = 1.835
$\frac{\rho_2}{\rho_1}$ = 1 + .04426u
τ = 48.6

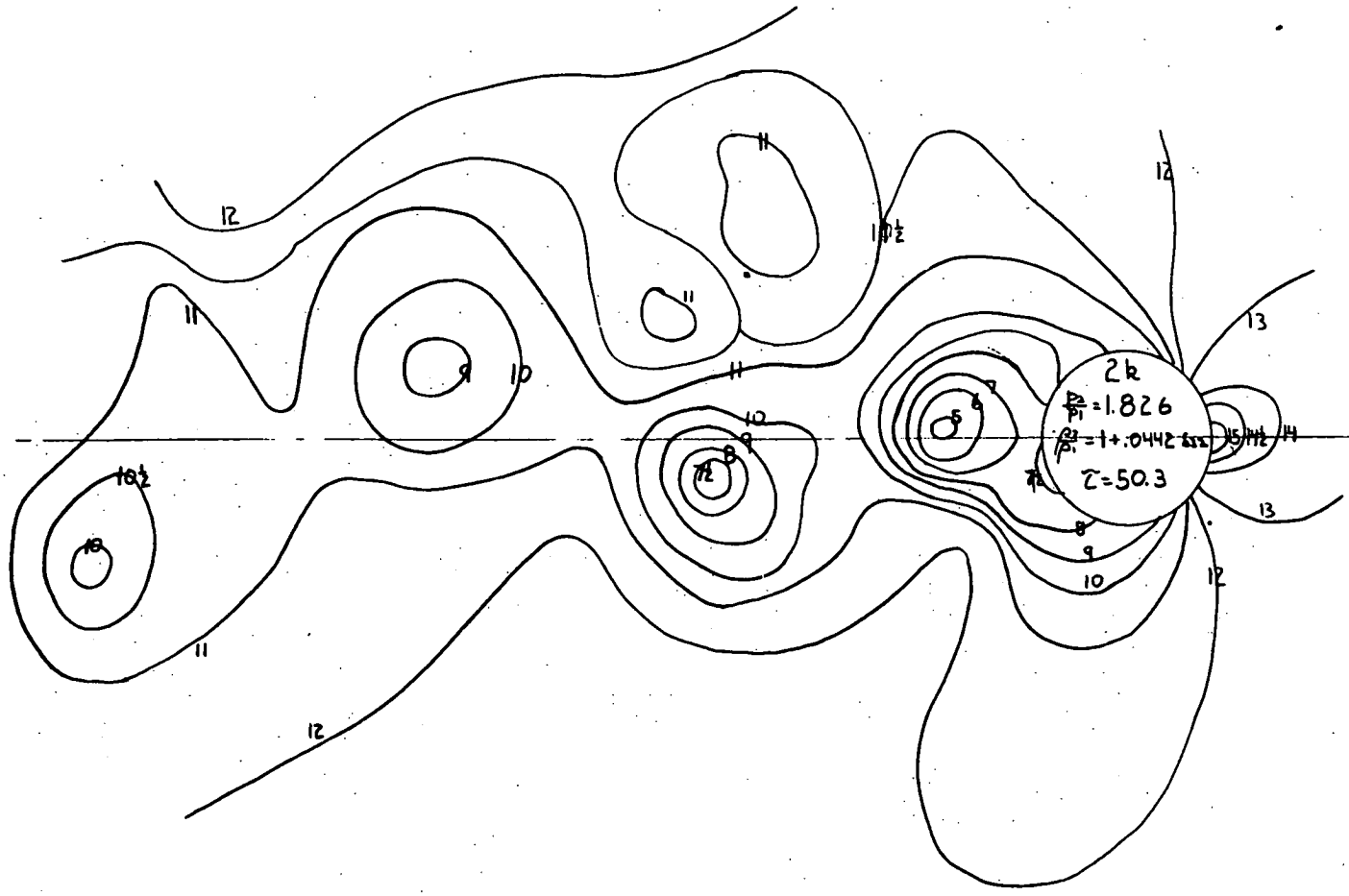
2k
$\frac{p_2}{p_1} = 1.826$
$\frac{\rho_2}{\rho_1} = 1 + .0442\,\delta_{21}$
$\tau = 50.3$

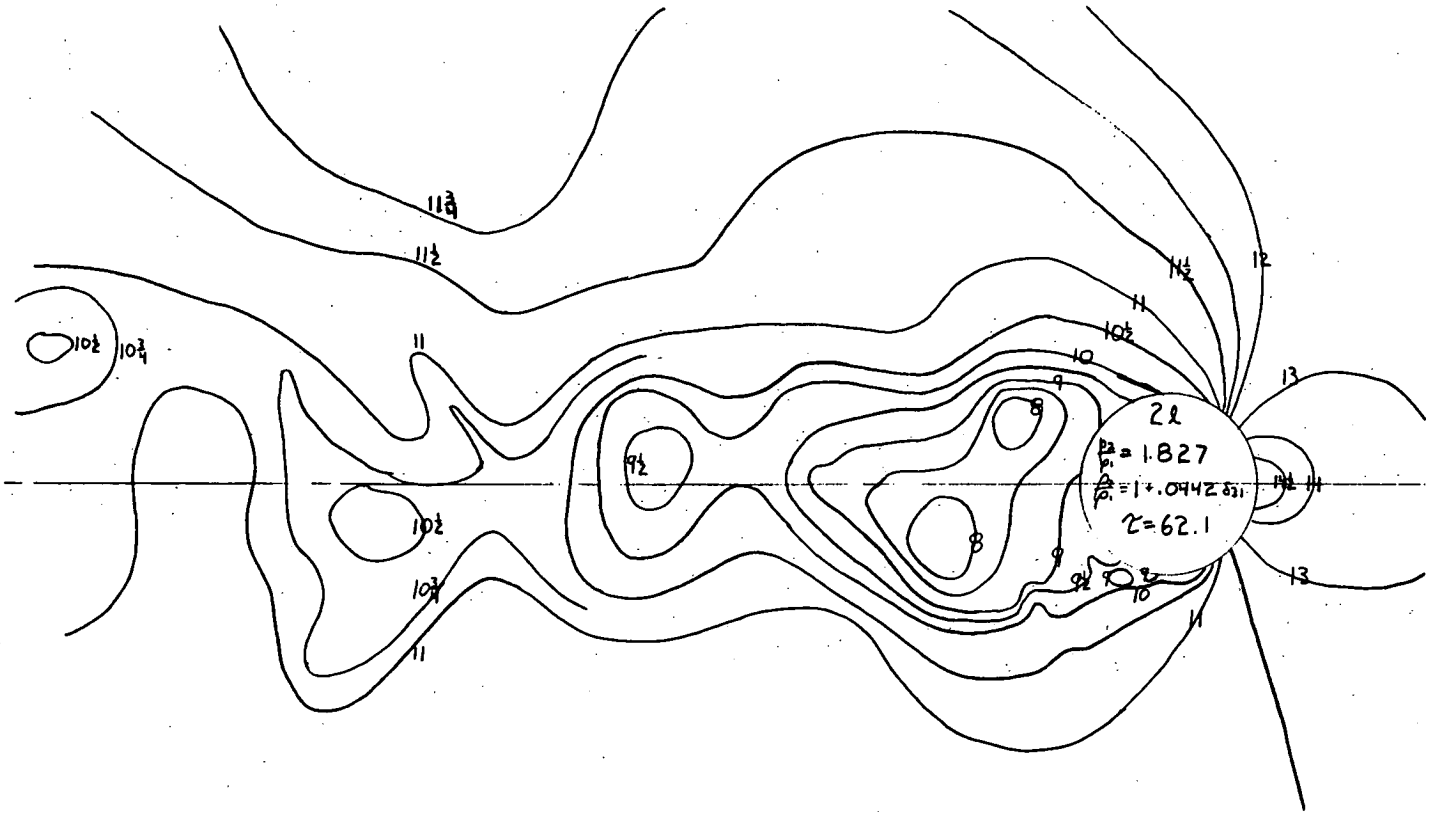
2ℓ
$\frac{p_2}{p_1} = 1.827$
$\frac{\rho_2}{\rho_1} = 1 + .0442\,\delta_{21}$
$\tau = 62.1$

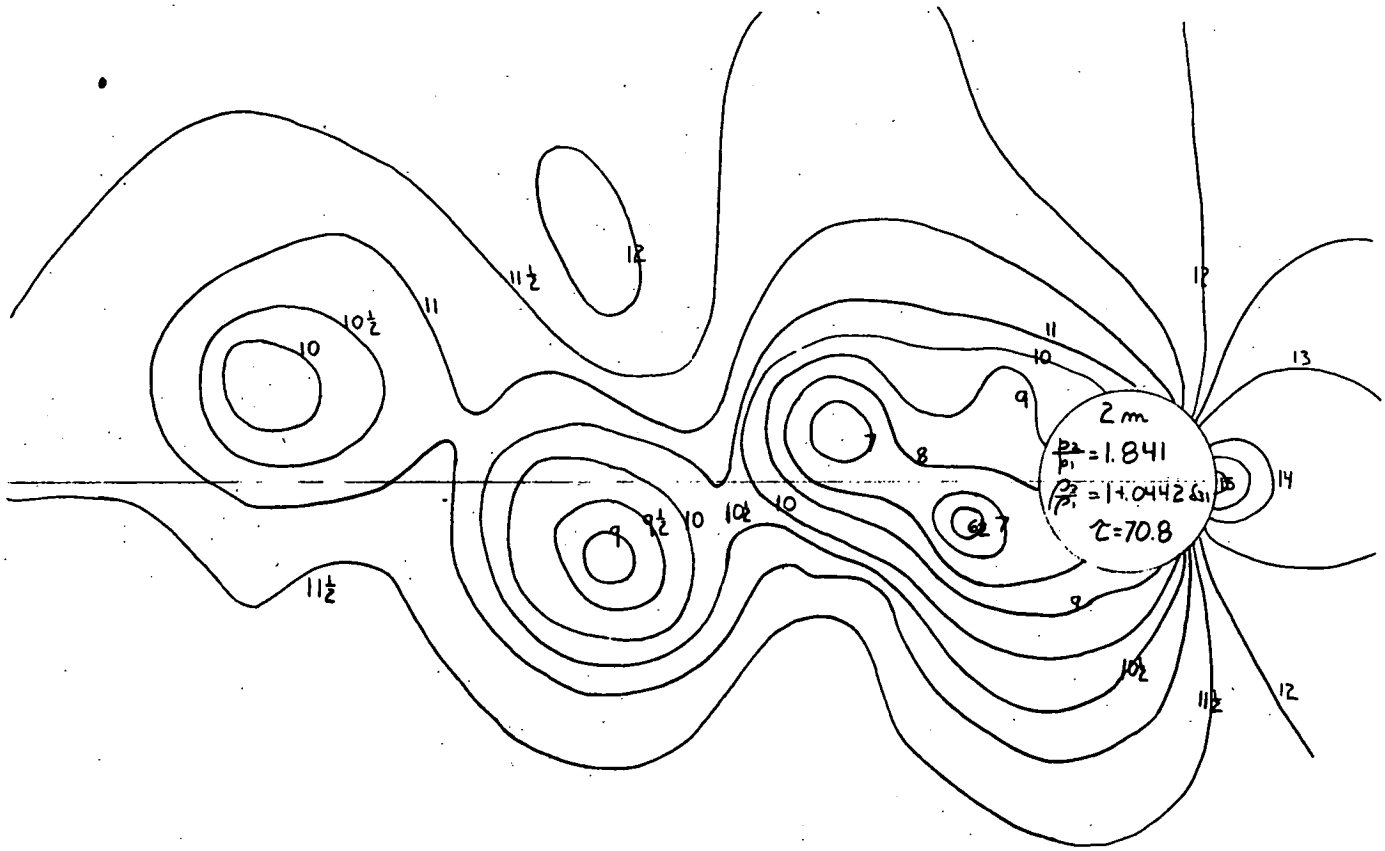
2 m
$\frac{p_2}{p_1}$ = 1.841
$\frac{\rho_2}{\rho_1}$ = 1+.0442 δ_{31}
τ = 70.8

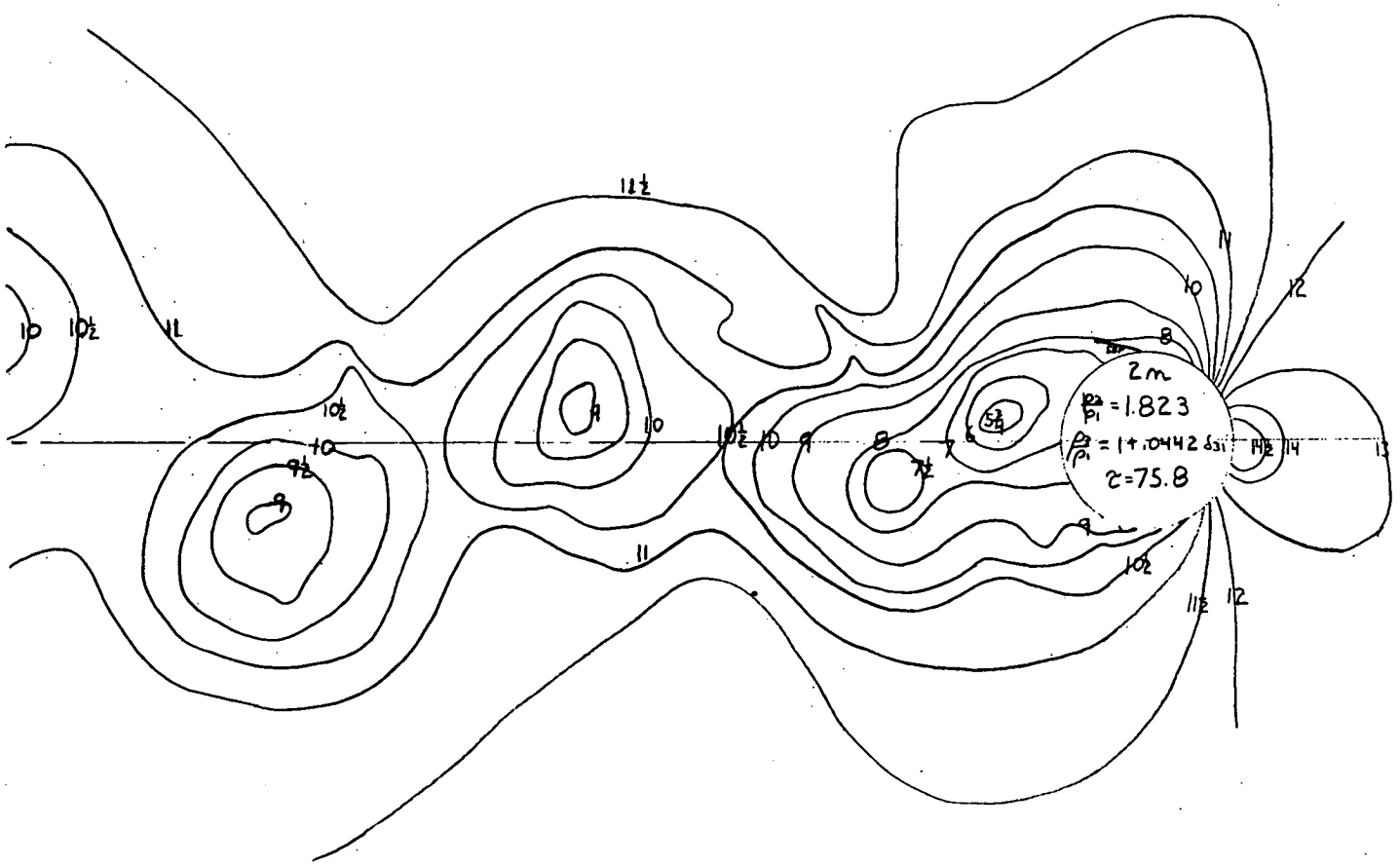
2 m
$\frac{p_2}{p_1}$ = 1.823
$\frac{\rho_2}{\rho_1}$ = 1+.0442 δ_{31}
τ = 75.8

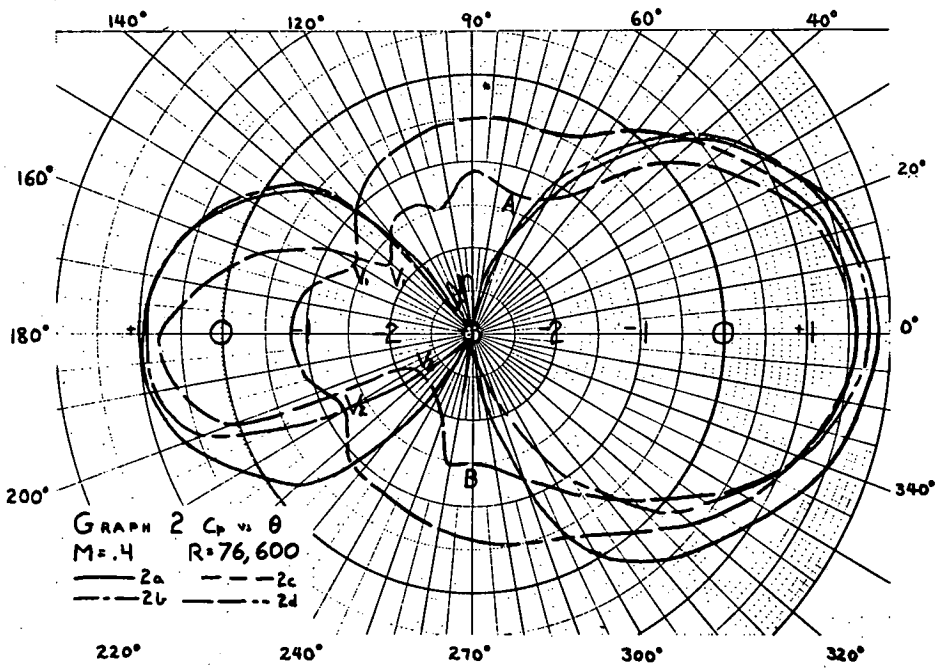
140°
120°
90°
60°
40°
160°
20°
180°
0°
200°
340°
220°
240°
270°
300°
320°
A
B
GRAPH 2 C_p vs θ
M=.4 R=76,600
2a
2b
2c
2d

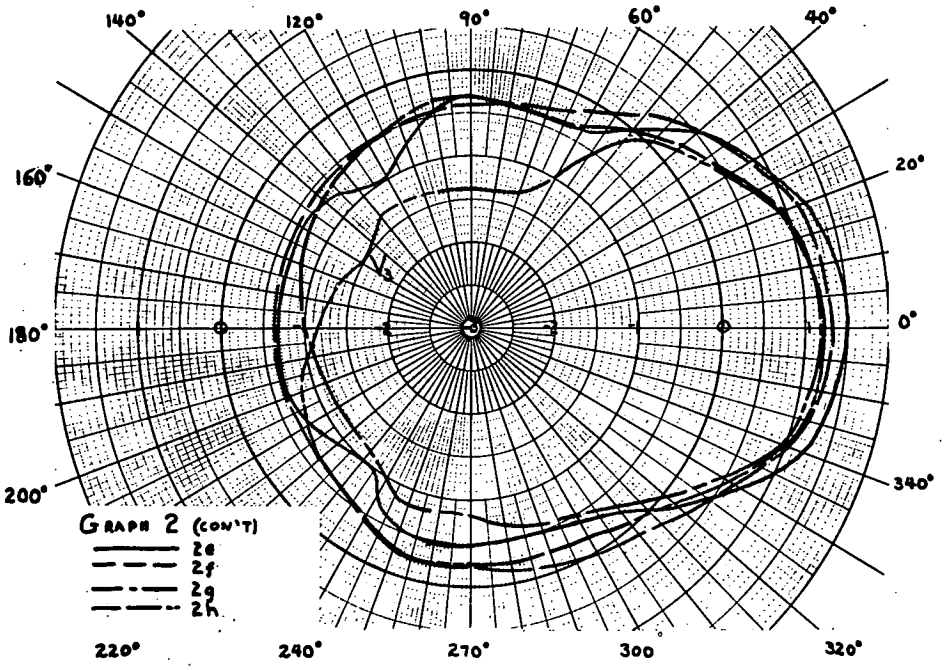
140°
120°
90°
60°
40°
160°
20°
180°
0°
200°
340°
220°
240°
270°
300
320°
GRAPH 2 (CON'T)
2e
2f
2g
2h

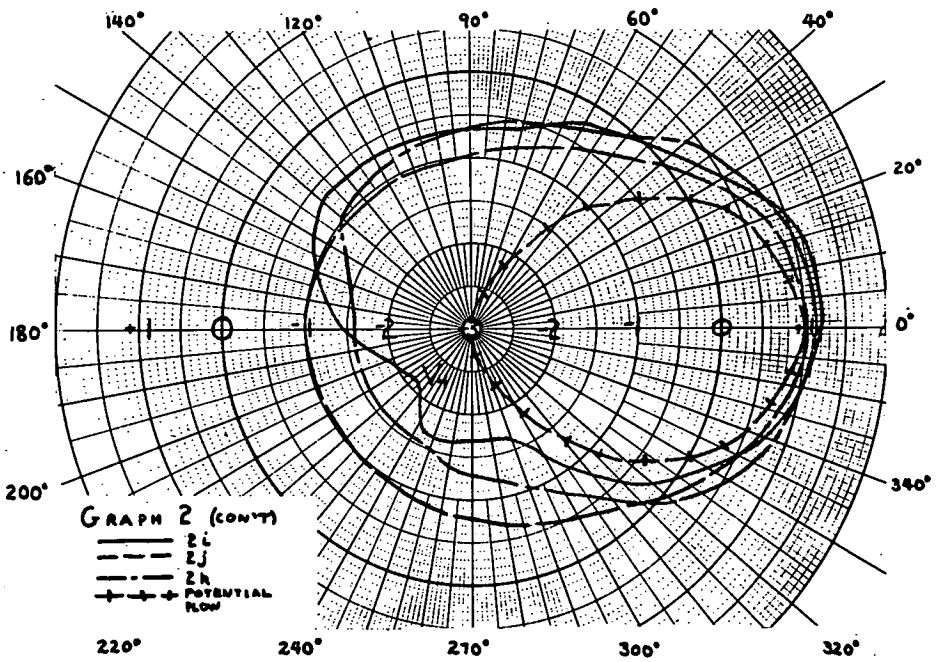
140°
120°
90°
60°
40°
160°
20°
180°
0°
200°
340°
220°
240°
270°
300°
320°
GRAPH 2 (CON'T)
2i
2j
2k
POTENTIAL FLOW

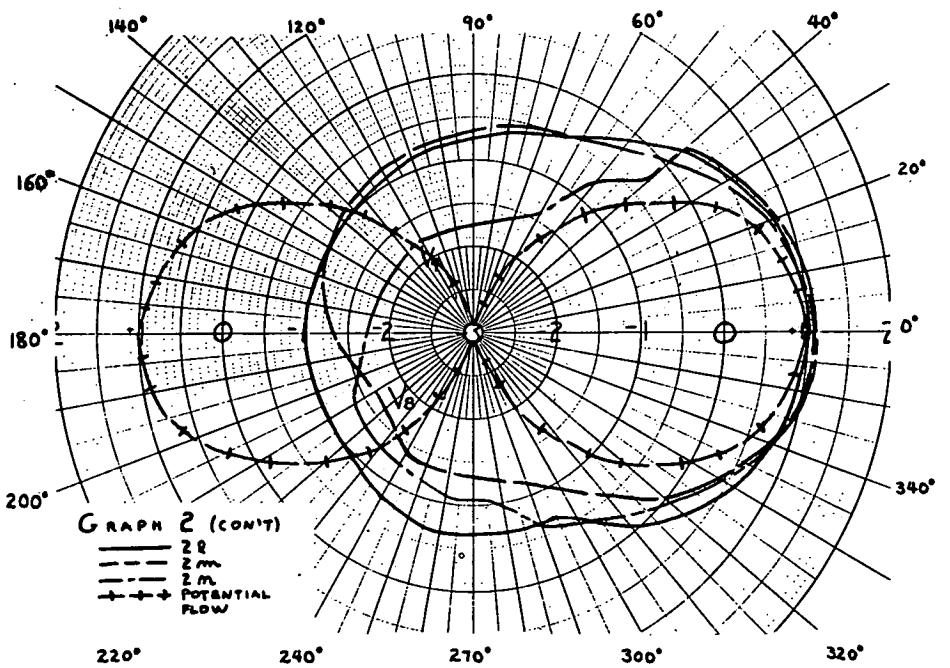
140°
120°
90°
60°
40°
160°
20°
180°
0°
200°
340°
220°
240°
270°
300°
320°
GRAPH 2 (CON'T)
2l
2m
2n
POTENTIAL FLOW

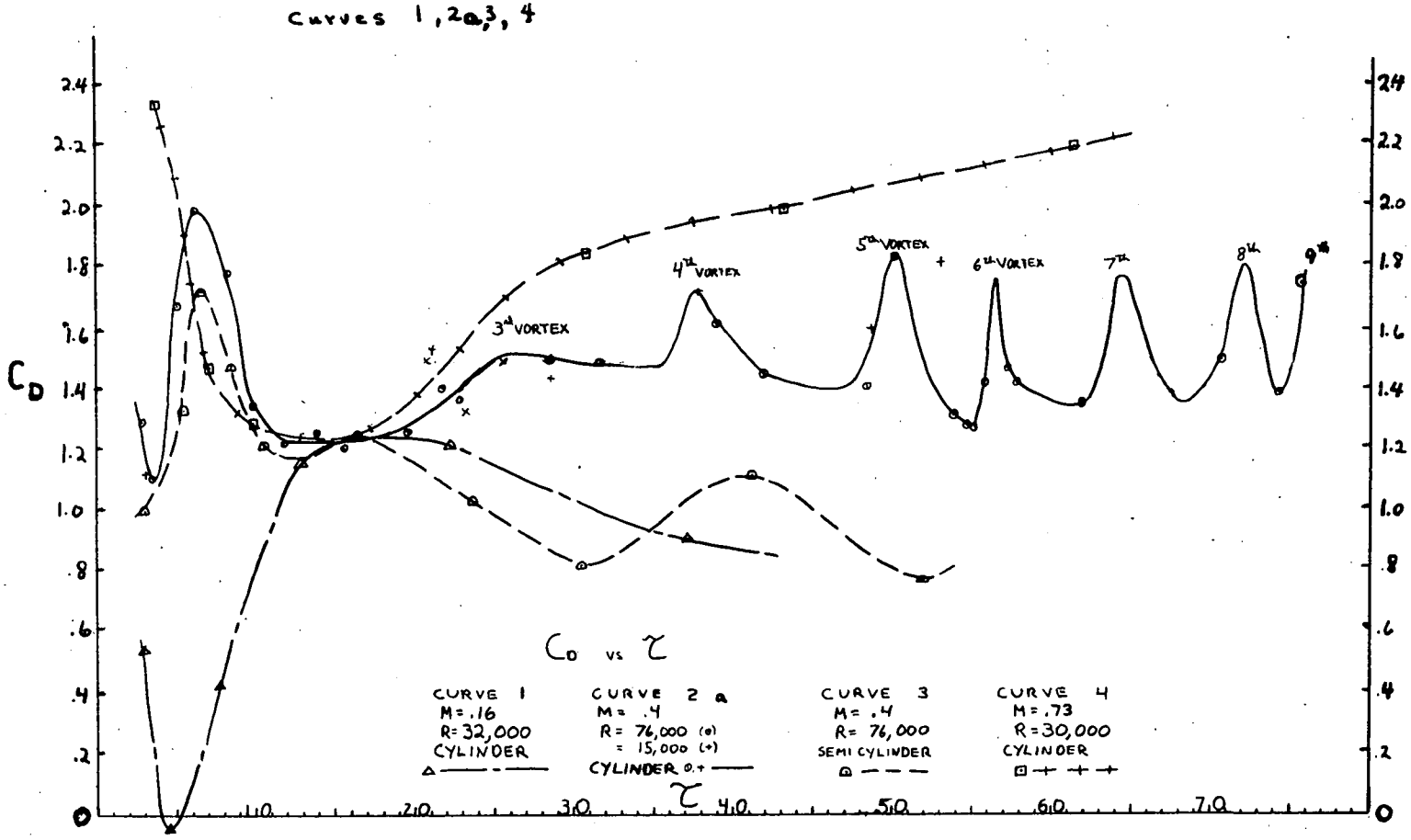
Curves 1, 2a, 3, 4
C_D
2.4
2.2
2.0
1.8
1.6
1.4
1.2
1.0
.8
.6
.4
.2
0
3rd VORTEX
4th VORTEX
5th VORTEX
6th VORTEX
7th
8th
9th
C_D vs τ
CURVE 1
M = .16
R = 32,000
CYLINDER
CURVE 2a
M = .4
R = 76,000 (o)
= 15,000 (+)
CYLINDER o,+
CURVE 3
M = .4
R = 76,000
SEMI CYLINDER
CURVE 4
M = .73
R = 30,000
CYLINDER
τ
1.0
2.0
3.0
4.0
5.0
6.0
7.0

Curve 2b

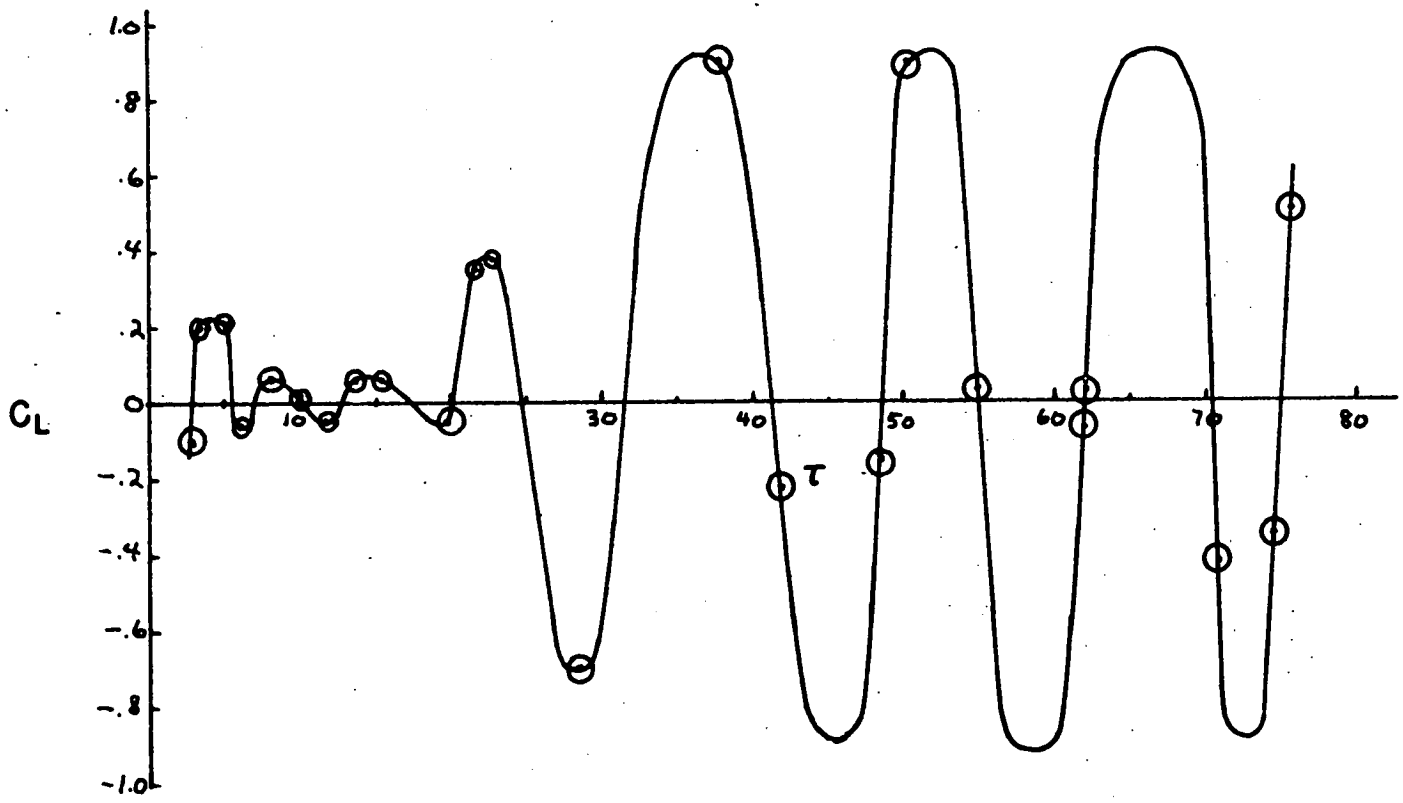

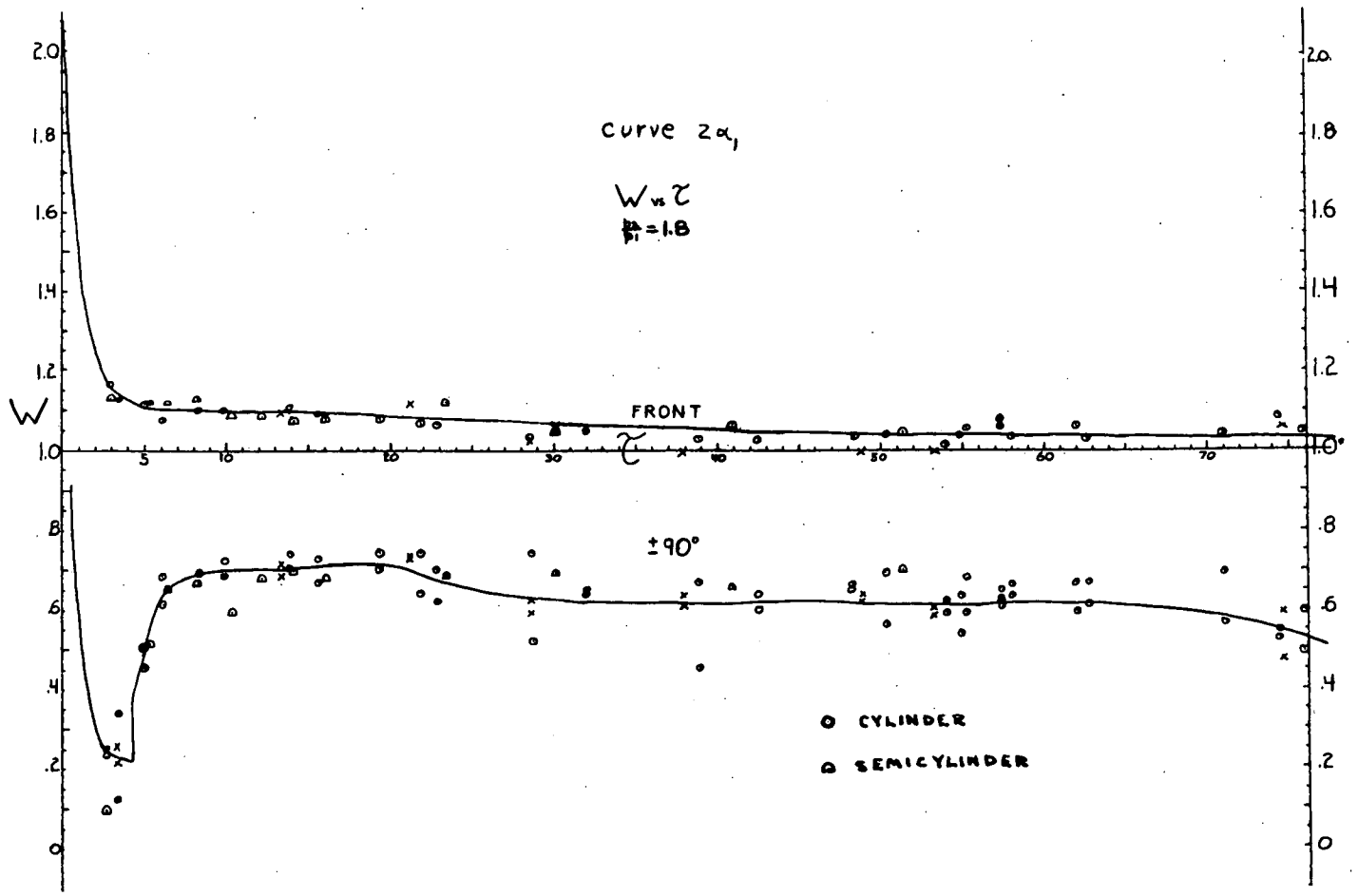
Curve 2α1
W vs τ
β1 = 1.8
W
τ
FRONT
±90°
CYLINDER
SEMICYLINDER
2.0
1.8
1.6
1.4
1.2
1.0
.8
.6
.4
.2
0
5
10
20
30
40
50
60
70

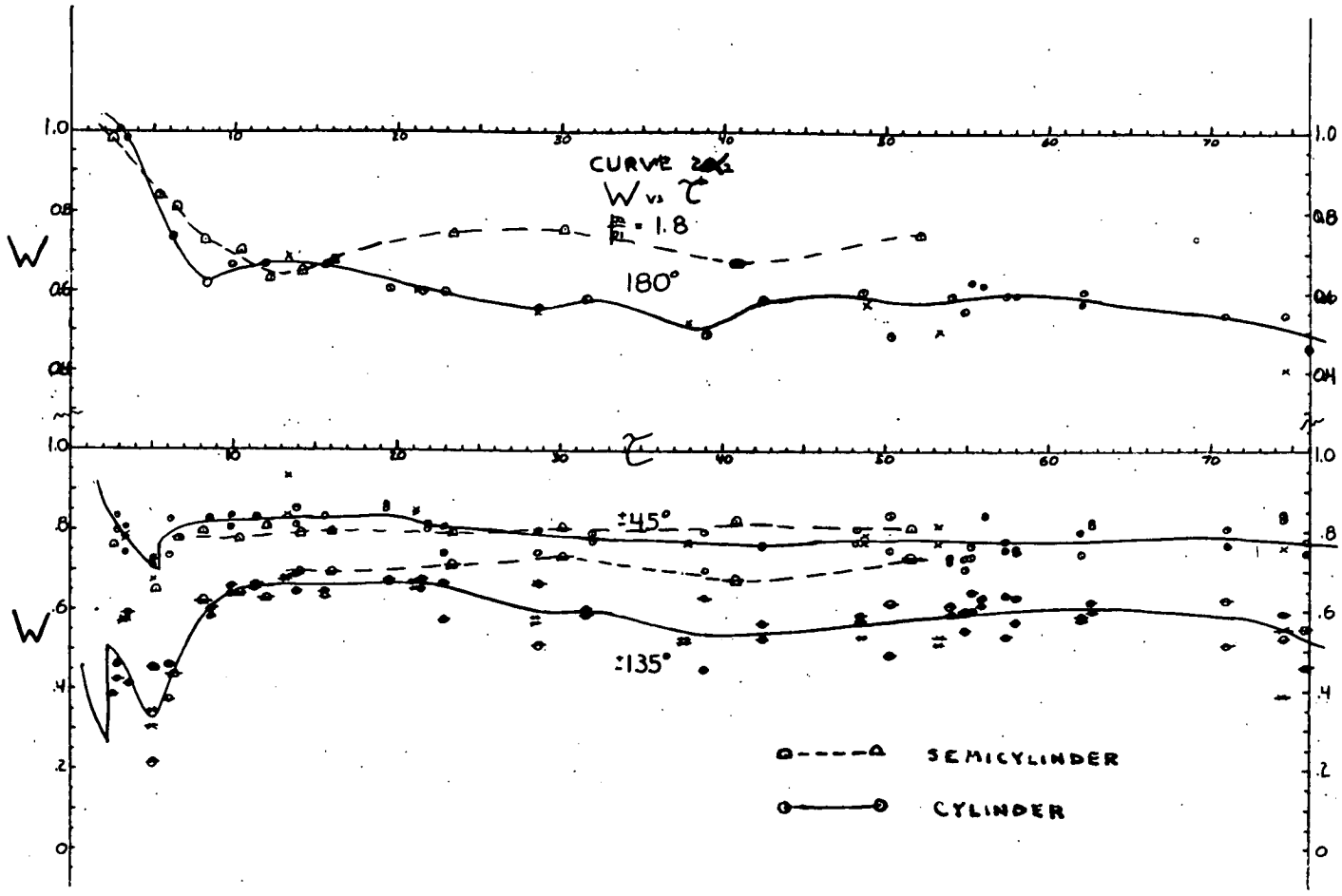
CURVE
W vs τ
= 1.8
180°
±45°
±135°
W
τ
SEMICYLINDER
CYLINDER

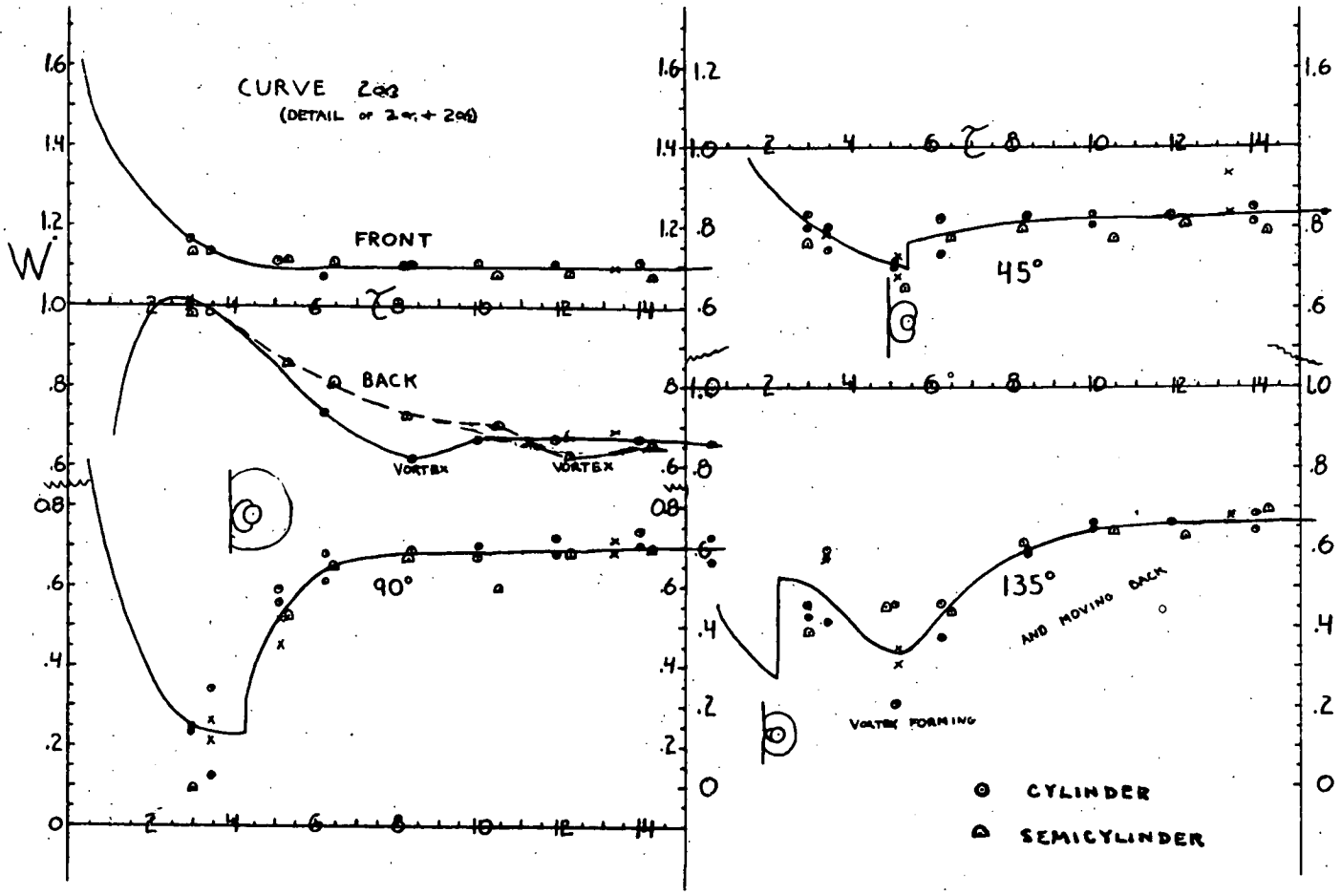
CURVE 203
(DETAIL OF 201 + 202)
W
FRONT
BACK
VORTEX
VORTEX
90°
45°
135°
AND MOVING BACK
VORTEX FORMING
CYLINDER
SEMICYLINDER

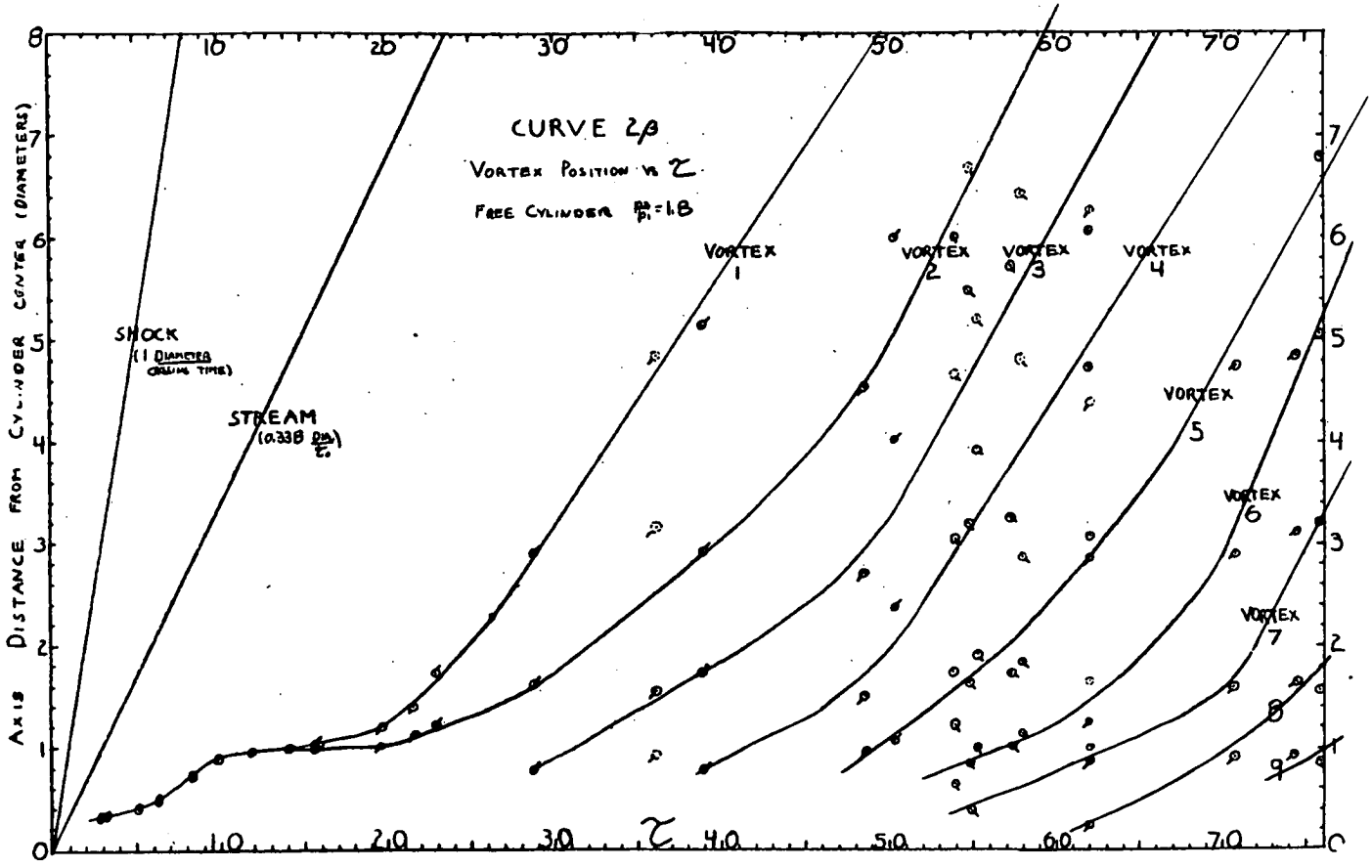
CURVE 2β
VORTEX POSITION VS τ
FREE CYLINDER p_b/p_t = 1.8
SHOCK
(1 DIAMETER / FREE STREAM TIME)
STREAM
(0.338 a_∞/D_c)
VORTEX 1
VORTEX 2
VORTEX 3
VORTEX 4
VORTEX 5
VORTEX 6
VORTEX 7
AXIS DISTANCE FROM CYLINDER CENTER (DIAMETERS)
τ
0
1.0
2.0
3.0
4.0
5.0
6.0
7.0
8
10
20
30
40
50
60
70

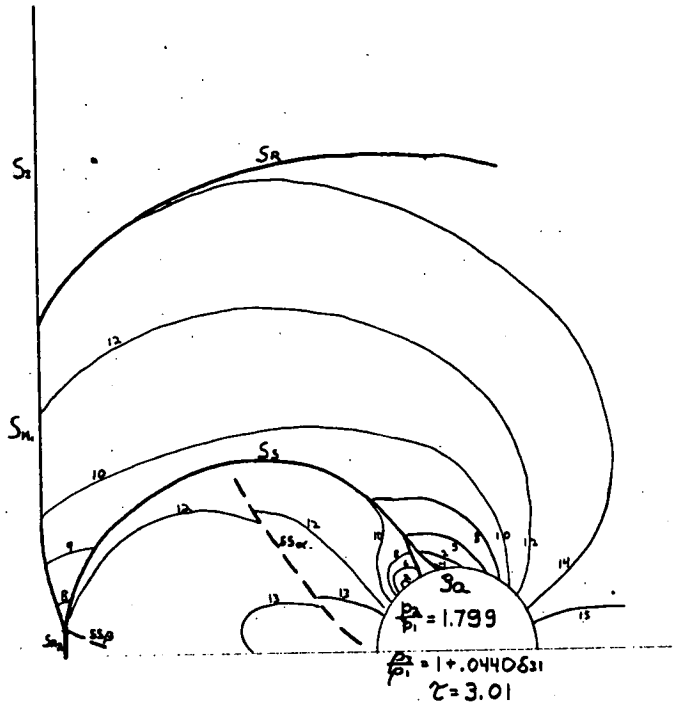
S_2
S_R
S_{M_1}
S_S
S_{M_2}
SSaft
SSar
S_a
$\frac{p_2}{p_1} = 1.799$
$\frac{\rho_2}{\rho_1} = 1 + .0440\delta_{31}$
$\tau = 3.01$

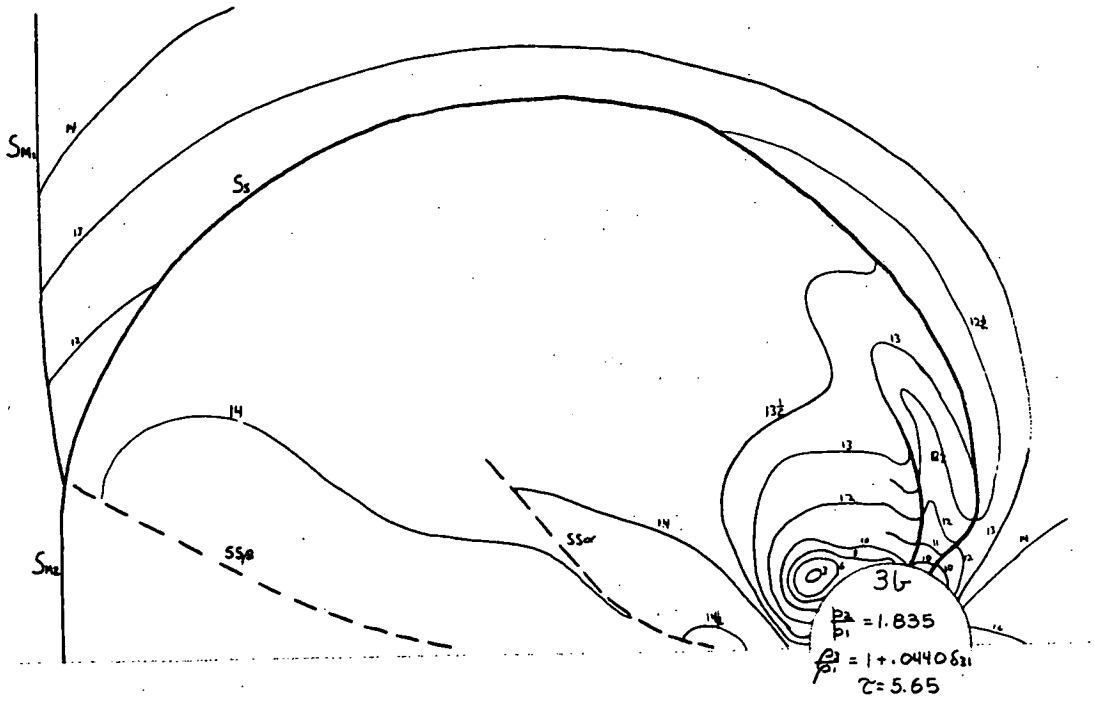
S_{M_1}
S_S
S_{M_2}
SSaft
SSar
3_b
$\frac{p_2}{p_1} = 1.835$
$\frac{\rho_2}{\rho_1} = 1 + .0440\delta_{31}$
$\tau = 5.65$

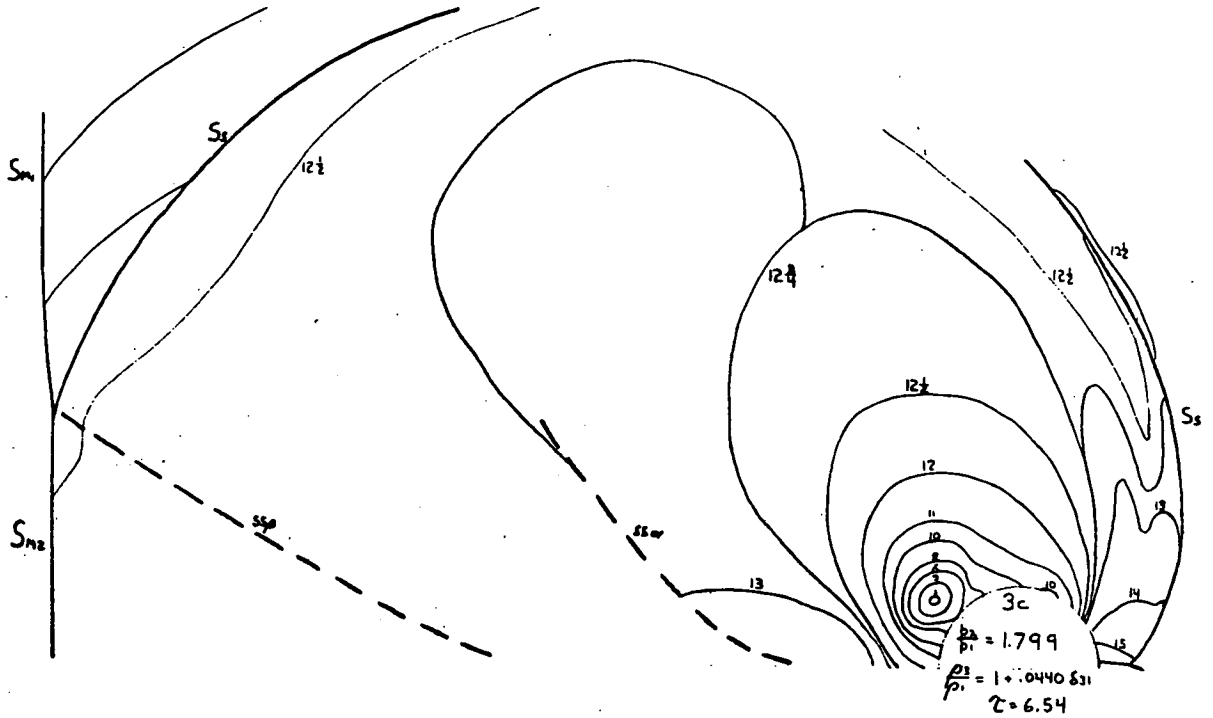
S_{m_1}
S_s
S_{m_2}
12½
12¾
13
14
15
3c
$\frac{\rho_2}{\rho_1}$ = 1.799
$\frac{\rho_3}{\rho_1}$ = 1 + .0440 δ31
τ = 6.54

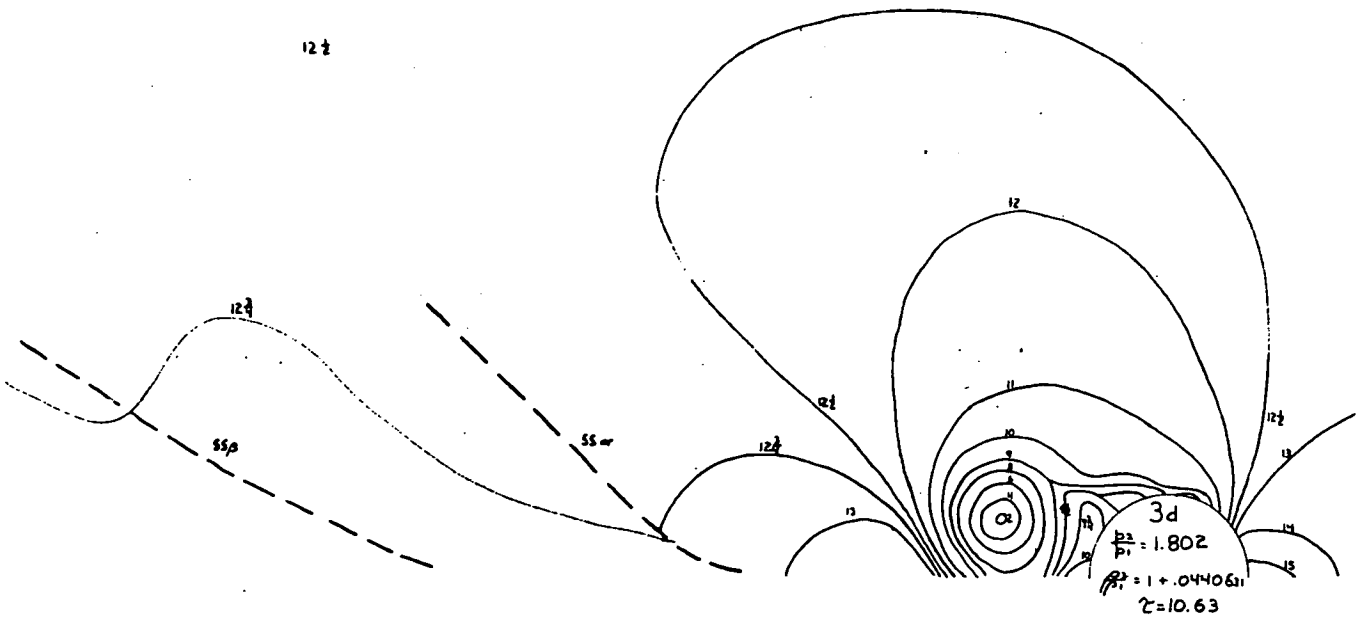
12½
12¾
13
14
15
3d
$\frac{\rho_2}{\rho_1}$ = 1.802
$\frac{\rho_3}{\rho_1}$ = 1 + .0440 δ31
τ = 10.63

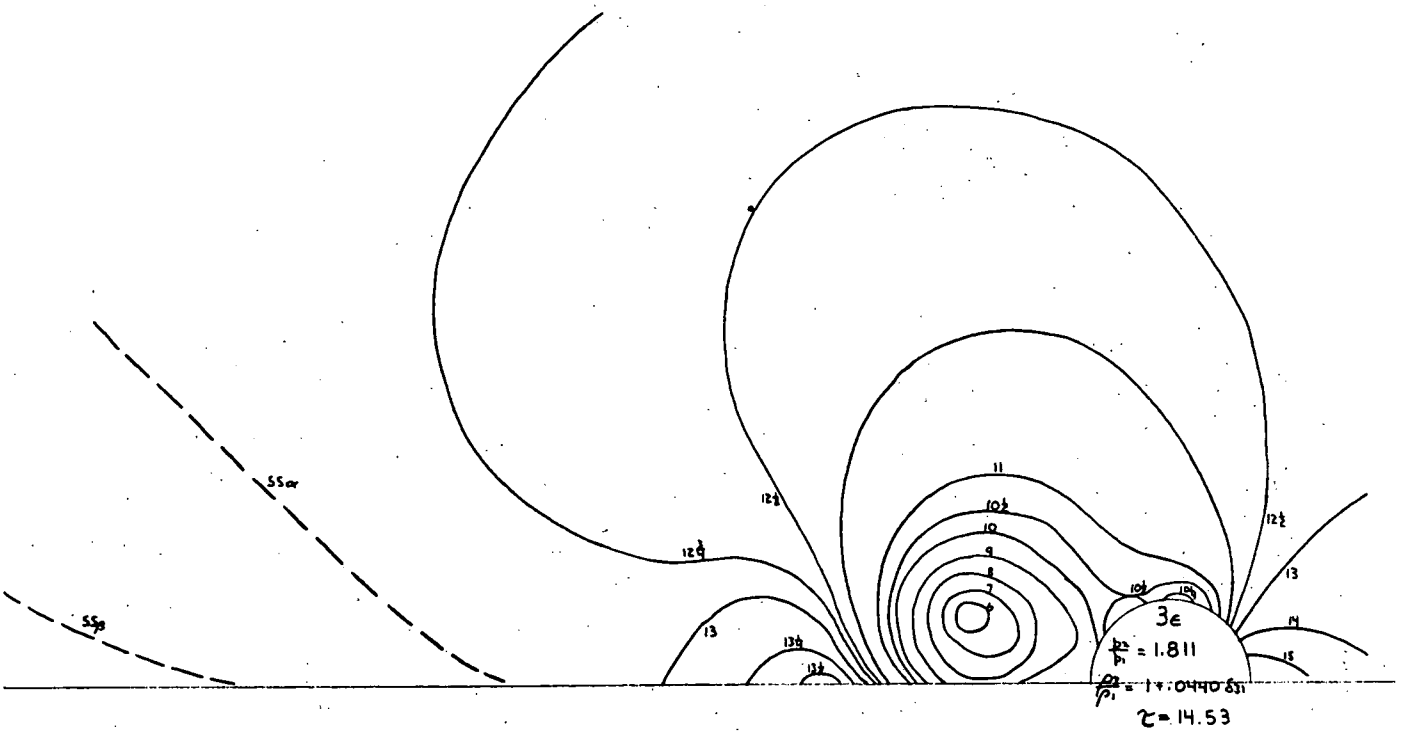
SSw
SSB
11
10½
10
9
8
7
6
12½
13
13½
3ε
$\frac{p_2}{p_1}$ = 1.811
$\frac{\rho_2}{\rho_1}$ = 1+.0440 δ_{31}
τ = 14.53

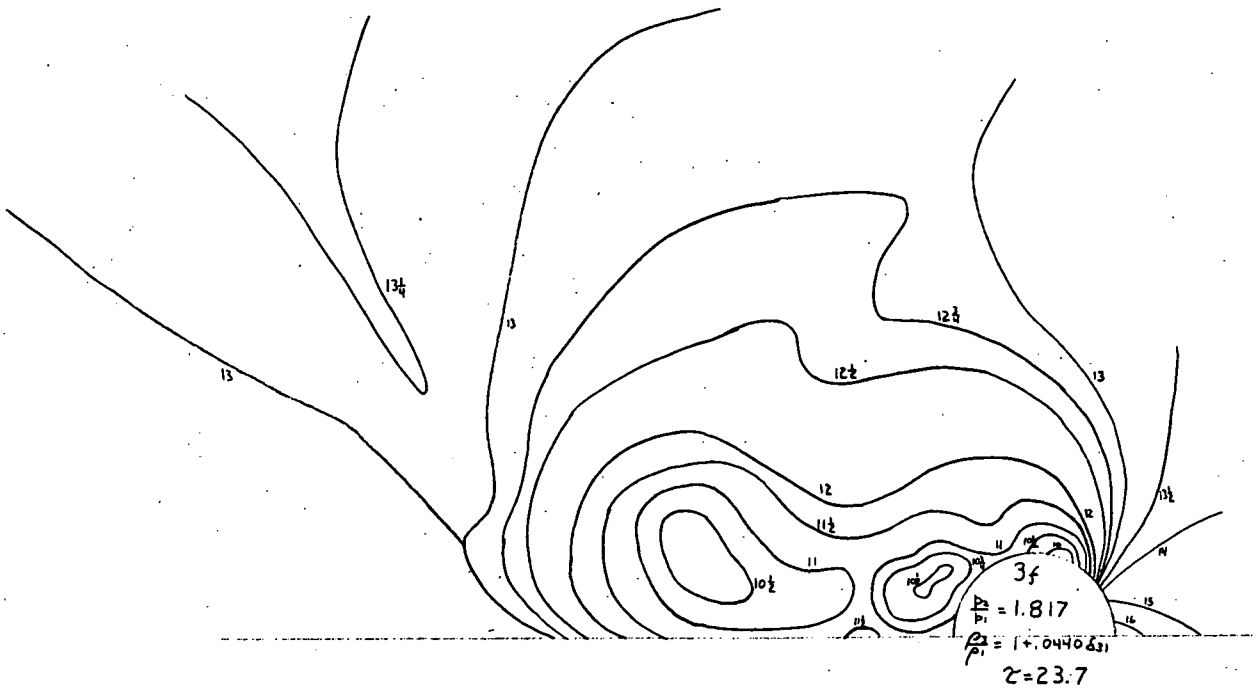
13½
13
13
12½
12½
13
12
11½
11
10½
3f
$\frac{p_2}{p_1}$ = 1.817
$\frac{\rho_2}{\rho_1}$ = 1+.0440 δ_{31}
τ = 23.7

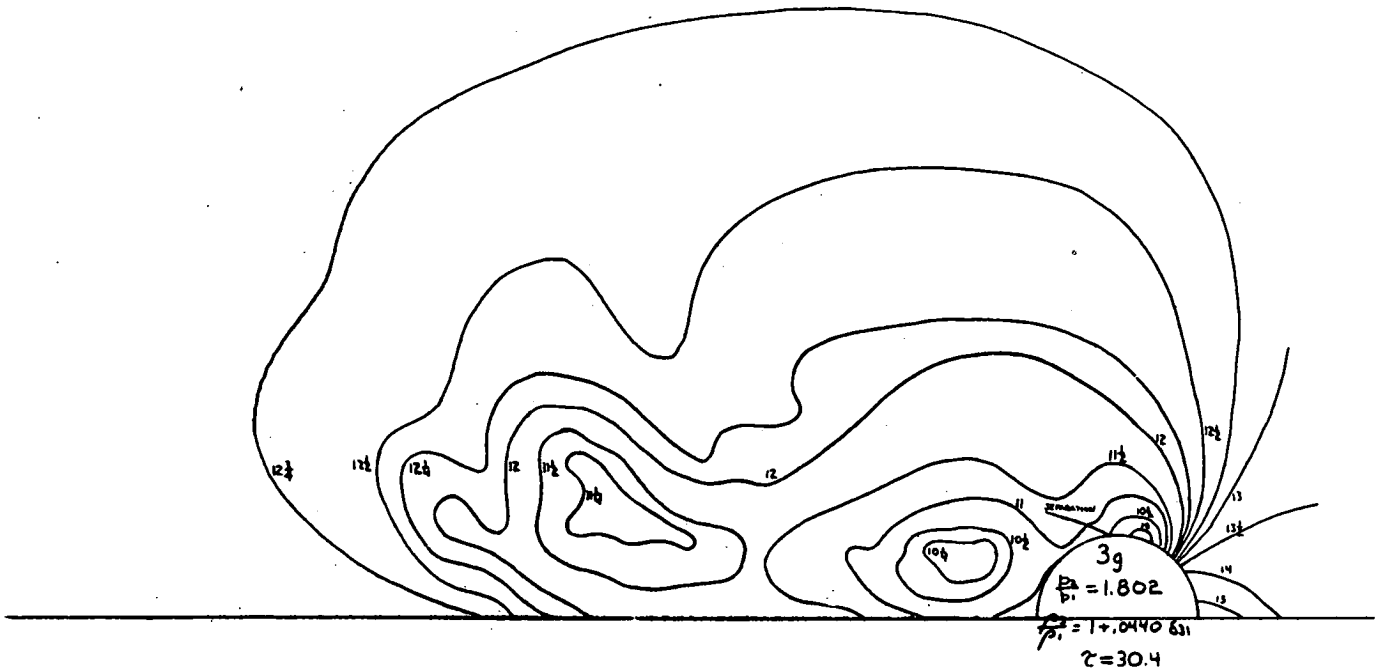
3g
$\frac{p_2}{p_1} = 1.802$
$\frac{p_2}{p_1} = 1 + .0440\,\delta_{31}$
$\tau = 30.4$

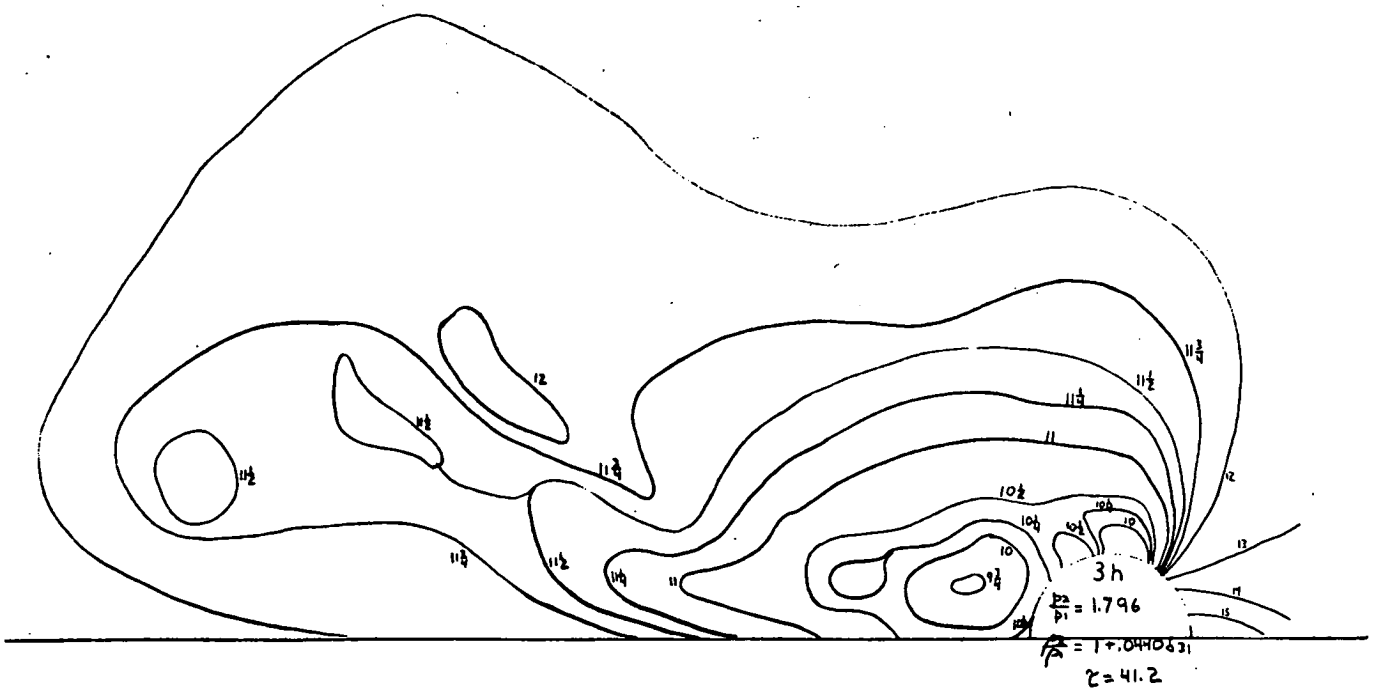
3h
$\frac{p_2}{p_1} = 1.796$
$\frac{p_2}{p_1} = 1 + .0440\,\delta_{31}$
$\tau = 41.2$

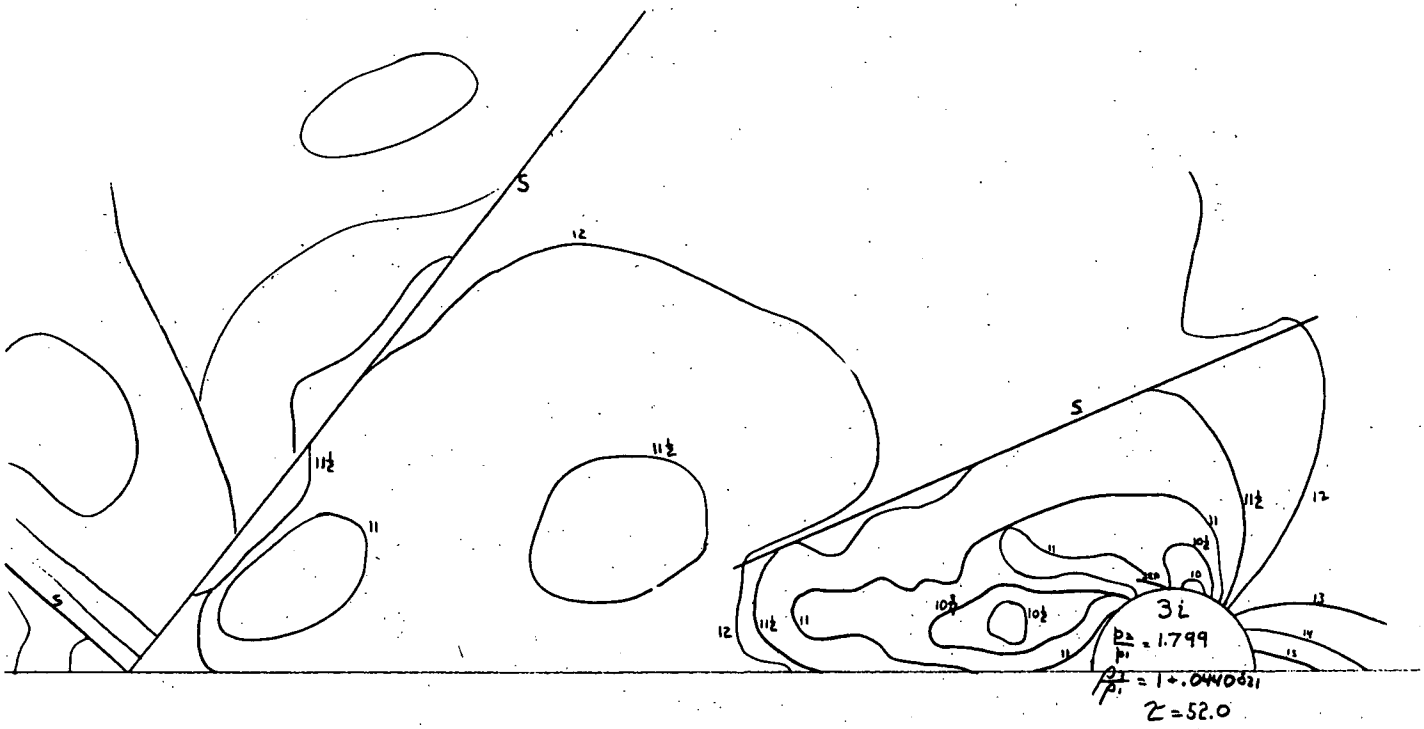
S
12
11½
11
S
11½
12
11½
11
10½
10
3i
$\frac{p_2}{p_1}$ = 1.799
$\frac{\rho_2}{\rho_1}$ = 1+.044 M_{n1}^2
Z = 52.0

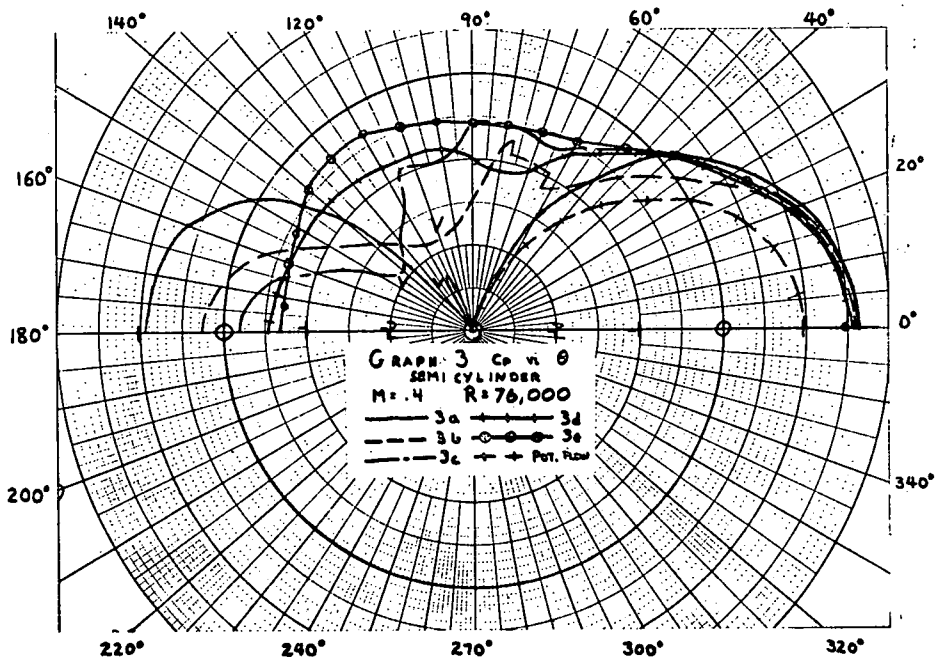
140°
120°
90°
60°
40°
160°
20°
180°
0°
200°
340°
220°
240°
270°
300°
320°
GRAPH 3 Cp vs θ
SEMI CYLINDER
M=.4 R=76,000
3a
3b
3c
3d
3e
POT. FLOW

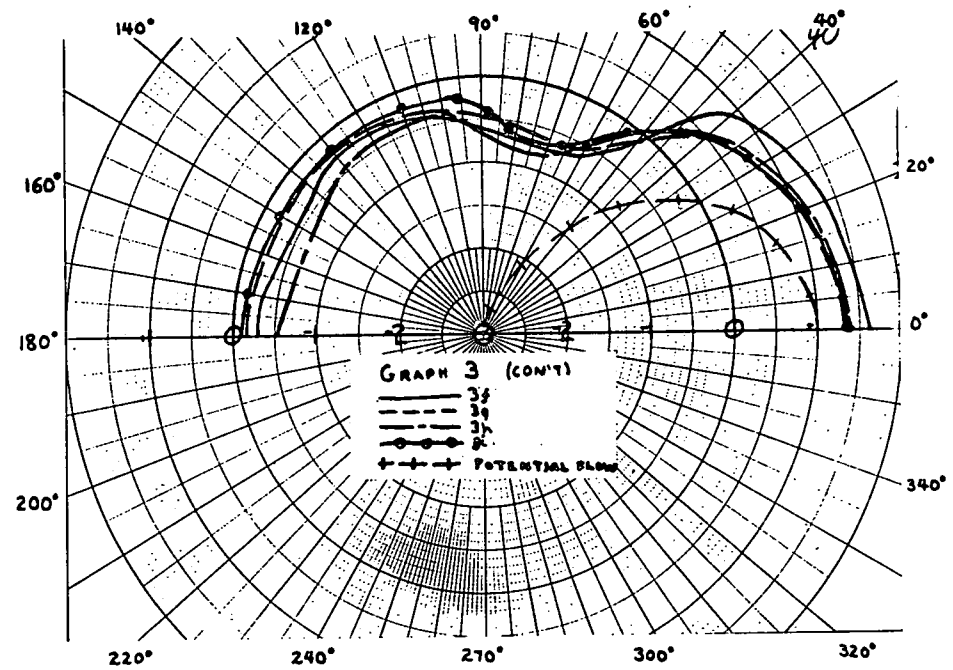
140°
120°
90°
60°
40°
160°
20°
180°
0°
200°
340°
220°
240°
270°
300°
320°
GRAPH 3 (CON'T)
3f
3g
3h
3i
POTENTIAL FLOW

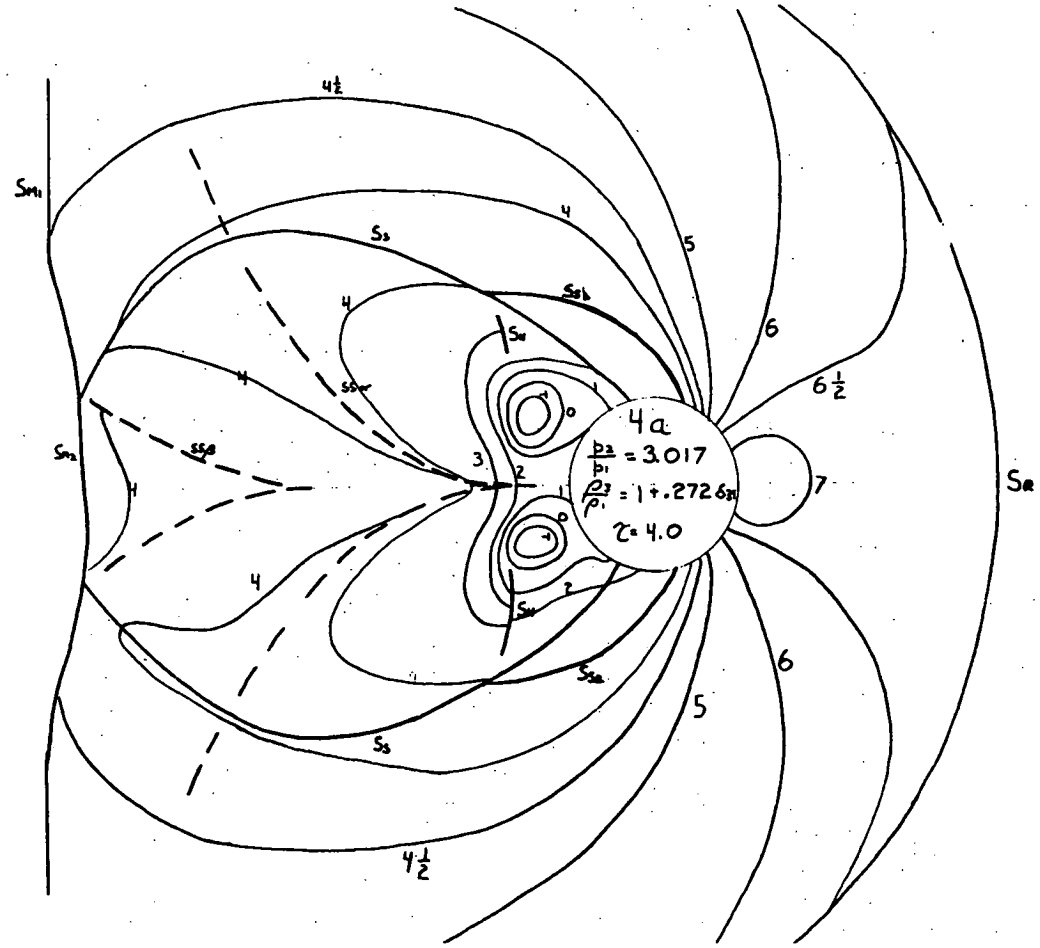
4a
$\frac{p_2}{p_1}$ = 3.017
$\frac{\rho_2}{\rho_1}$ = 1+.272 631
τ = 4.0
S_{M_1}
S_{M_2}
S_3
S_{sb}
S_{sa}
S_a
ssa
ssb
4½
5
6
6½
7

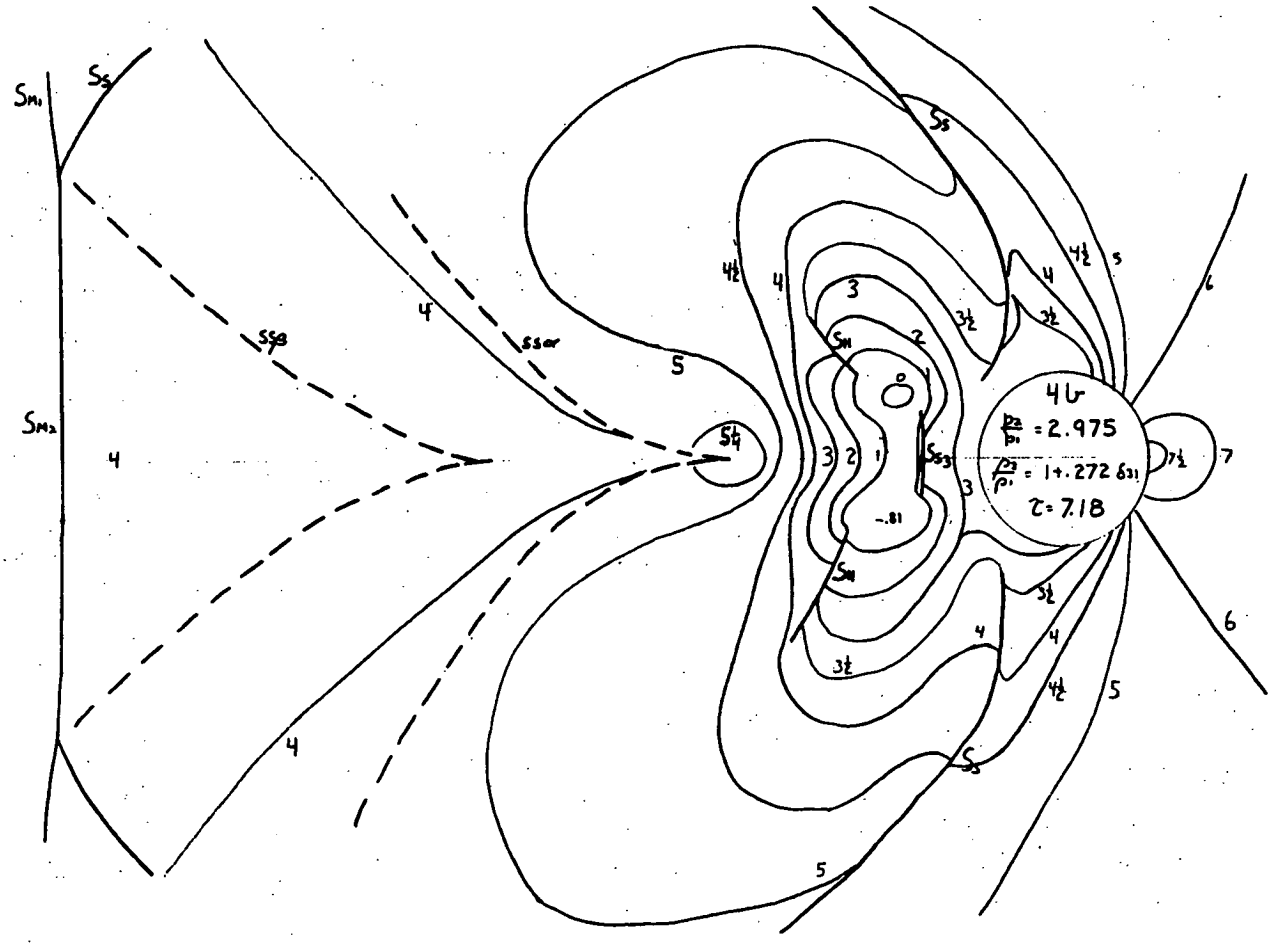
4b
$\frac{p_2}{p_1}$ = 2.975
$\frac{\rho_2}{\rho_1}$ = 1+.272 631
τ = 7.18
S_{M_1}
S_{M_2}
S_3
S_{sb}
S_{sa}
S_{s3}
ssa
ssb
-.81
4½
5
6
7½

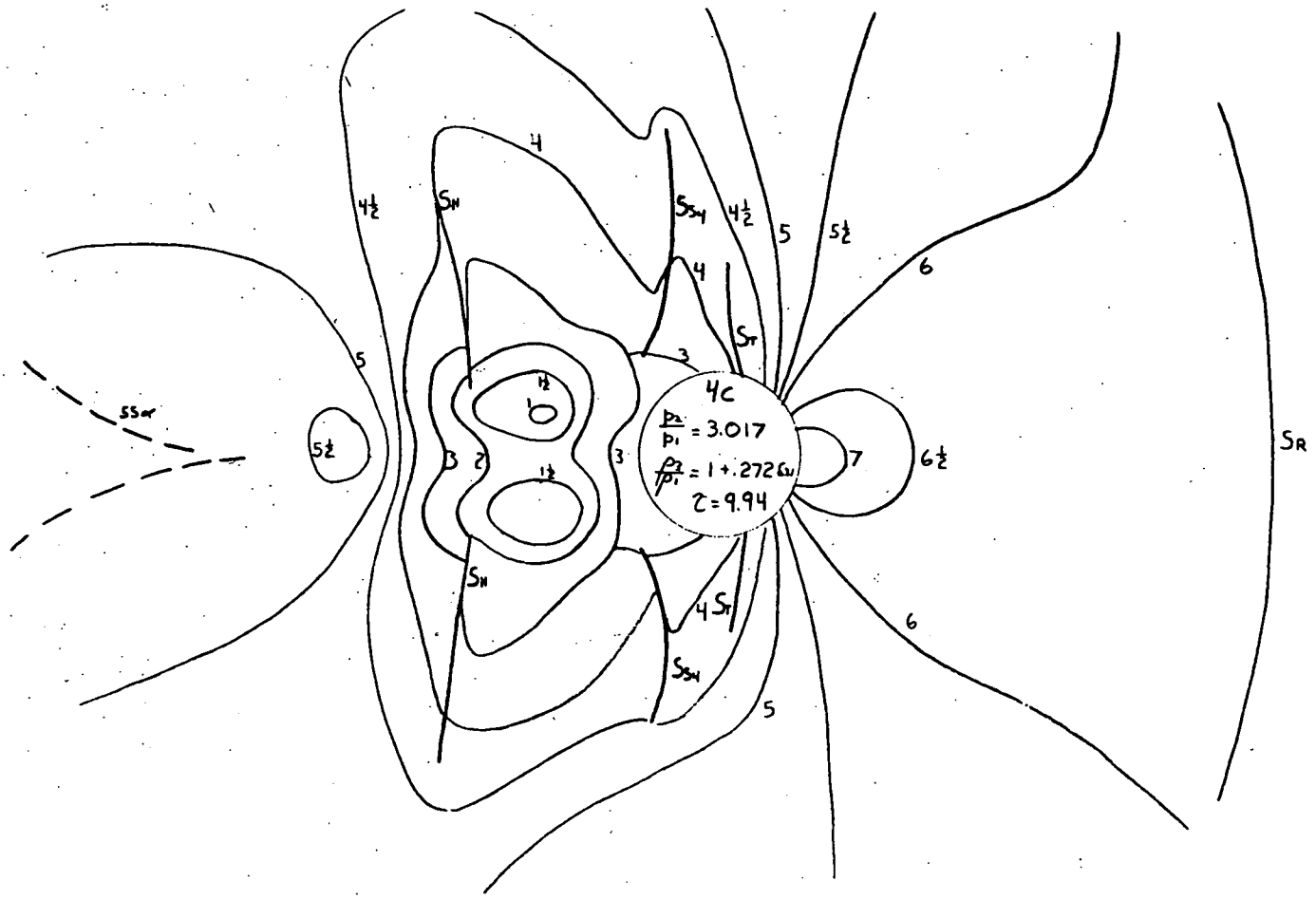
4c
$\frac{\rho_2}{\rho_1} = 3.017$
$\frac{\rho_3}{\rho_1} = 1 + .272\omega_1$
$\tau = 9.94$
S_M
S_{SM}
S_T
S_R
SSM

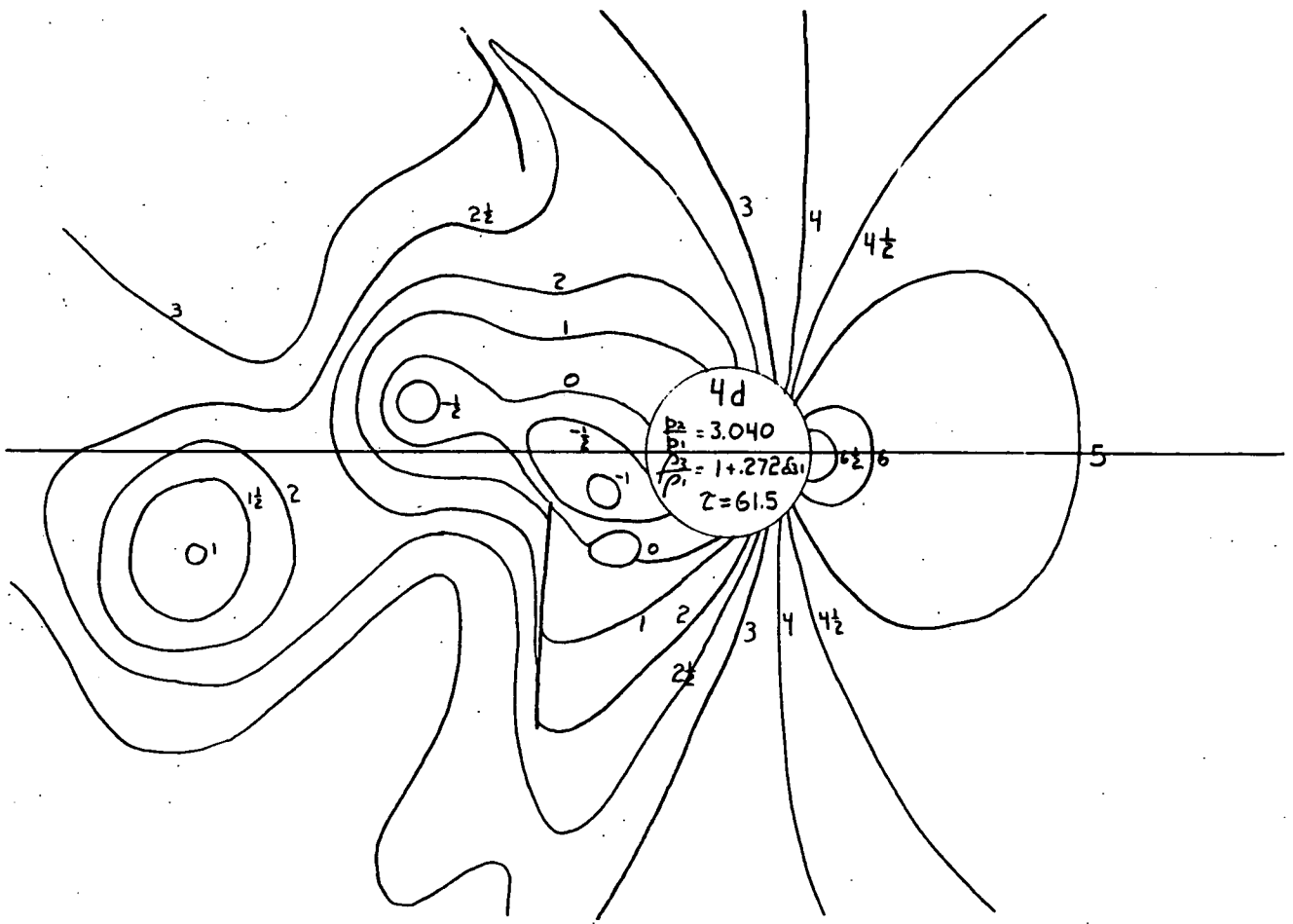
4d
$\frac{\rho_2}{\rho_1} = 3.040$
$\frac{\rho_3}{\rho_1} = 1 + .272\omega_1$
$\tau = 61.5$

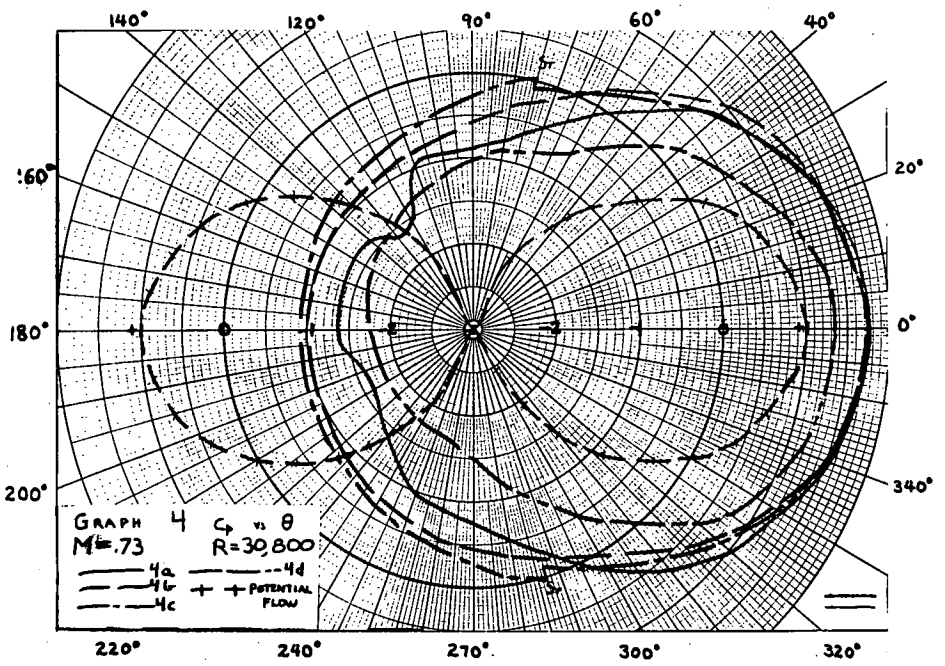
140°
120°
90°
60°
40°
160°
20°
180°
0°
200°
340°
220°
240°
270°
300°
320°
GRAPH 4 C_p vs θ
M=.73
R=30,800
4a
4b
4c
4d
POTENTIAL FLOW